# REPORT DOCUMENTATION PAGE

Form Approved
OMB NO. 0704-0188



| 1. AGENCY USE ONLY ( Leave Blank) | 2. REPORT DATE | 3. REPORT TYPE AND DATES COVERED |
|---|---|---|
| | 08-30-2005 | Final Technical Report<br>Feb. 15, 2005 - August 15, 2005 |

4. TITLE AND SUBTITLE
Continuous Hypergolic Monitor Network for Shipboard Applications

5. FUNDING NUMBERS
W9113M-05-C-0100

6. AUTHOR(S)
Todd, Mlnsa

7. PERFORMING ORGANIZATION NAME(S) AND ADDRESS(ES)
Seacoast Science, Inc.
2151 Las Palmas Drive Suite C, Carlsbad, CA 92011

8. PERFORMING ORGANIZATION

9. SPONSORING / MONITORING AGENCY NAME(S) AND ADDRESS(ES)

U. S. Army Space and Missile Defense Command
SMDC – CM-AK, Jackson
PO BOX 1500
Huntsville, AL 35807-3801

10. SPONSORING / MONITORING AGENCY REPORT NUMBER

11. SUPPLEMENTARY NOTES
The views, opinions and/or findings contained in this report are those of the author(s) and should not be construed as an official Department of the Army position, policy or decision, unless so designated by other documentation.

12 a. DISTRIBUTION / AVAILABILITY STATEMENT

Approved for public release; distribution unlimited.

12 b. DISTRIBUTION CODE

13. ABSTRACT (Maximum 200 words)

Report developed under SBIR contract" for topic "MDA04-146"

This report was developed under SBIR contract for topic MDA04-146. Seacoast Science, Inc. has provided proof-of-concept technical results and proposed prototype design for the detection of hypergolic fuels and oxidizers for use in the MDA Kinetic Energy Interceptor (KEI) program. The proposed sensor system consists of three different sensor cases all containing a MEMS chemicapacitor sensor array. Seacoast's sensor technology utilizes an array of micromachined capacitors, coated with chemoselective materials selected for their sensitivity to the hypergolic fuels and oxidizers.

We have successfully accomplished the primary objective of this Phase I program by establishing the viability of Seacoast Science's capacitive sensors to detect hypergolic chemicals (monomethyl hydrazine) at a concentration well below its LEL level and within 2 orders of magnitude of its PEL with first generation selective materials. First generation sensors have also demonstrated detection of oxidizer off-gas ($NO_2$) two orders of magnitude below its PEL. In addition the following project tasks were completed: 1) New chemosensitive materials were synthesized and characterized. 2) Motherboard was redesigned to decrease power consumption and size. 3) Pattern recognition program was initiated for incorporation into a Phase II product. 4) Completed design of prototype sensor suite for fuel detection in the KEI program.

| 14. SUBJECT TERMS | 15. NUMBER OF PAGES |
|---|---|
| SBIR Report | 28 |
| | 16. PRICE CODE |

| 17. SECURITY CLASSIFICATION OR REPORT | 18. SECURITY CLASSIFICATION ON THIS PAGE | 19. SECURITY CLASSIFICATION OF ABSTRACT | 20. LIMITATION OF ABSTRACT |
|---|---|---|---|
| **UNCLASSIFIED** | **UNCLASSIFIED** | **UNCLASSIFIED** | **UL** |

# Report Documentation Page

*Form Approved*
*OMB No. 0704-0188*



| 1. REPORT DATE | 2. REPORT TYPE | 3. DATES COVERED |
|---|---|---|
| **30 MAR 2005** | **N/A** | **-** |

| 4. TITLE AND SUBTITLE | 5a. CONTRACT NUMBER |
|---|---|
| **Continuous Hypergolic Monitor Network for Shipboard Applications** | **W9113M-05-C-0100** |
| | 5b. GRANT NUMBER |
| | 5c. PROGRAM ELEMENT NUMBER |
| 6. AUTHOR(S) | 5d. PROJECT NUMBER |
| | 5e. TASK NUMBER |
| | 5f. WORK UNIT NUMBER |
| 7. PERFORMING ORGANIZATION NAME(S) AND ADDRESS(ES) **Seacoast Science, Inc., 2151Las Palmas Drive, Suite C, Carlsbad, CA 92011** | 8. PERFORMING ORGANIZATION REPORT NUMBER |
| 9. SPONSORING/MONITORING AGENCY NAME(S) AND ADDRESS(ES) | 10. SPONSOR/MONITOR'S ACRONYM(S) |
| | 11. SPONSOR/MONITOR'S REPORT NUMBER(S) |

12. DISTRIBUTION/AVAILABILITY STATEMENT
**Approved for public release, distribution unlimited**

13. SUPPLEMENTARY NOTES
**The original document contains color images.**

14. ABSTRACT

15. SUBJECT TERMS

| 16. SECURITY CLASSIFICATION OF: | | | 17. LIMITATION OF ABSTRACT | 18. NUMBER OF PAGES | 19a. NAME OF RESPONSIBLE PERSON |
|---|---|---|---|---|---|
| a. REPORT | b. ABSTRACT | c. THIS PAGE | | | |
| **unclassified** | **unclassified** | **unclassified** | **UU** | **29** | |

Final Report on the Small Business Innovation Research (SBIR) project entitled
"***Chemicapacitive Hypergolic Chemical Detector System***"
Topic # **MDA04-146**: Contractor: Seacoast Science, Inc.: Contract Number W9113M-05-C-0100
Period of Performance: 15 February 2005 – 15 August 2005

**Purpose of the Research:** There is a growing threat of foreign enemy states and terrorist organizations acquiring ballistic missile technology to use or threaten to use against the United State or our allies. Because of the instability of certain rogue nations and terrorist agents, the threat of massive retaliation may not be a sufficient deterrent. Part of the MDA's proposed protection scheme is the Kinetic Energy Interceptor (KEI) to be used in the Boost Phase Defense. For the KEI system, the ideal missile design uses a liquid fuel initiatior (monomethyl hydrazine – fuel; nitrogen tetroxide – oxidizer). The overarching goal of this project is to satisfy the concerns of the current policy of the United States Navy (USN) that prohibits these chemicals on USN vessels. A detection system that addresses the concerns of the USN both from the possible explosion danger and the toxic adverse effects from MMH would assist in this process. Seacoast Science proposes a chemical sensor suite based on microelectromechanical capacitor technology that will allow for alarm detection of high levels (LEL) of hypergolic compounds within the canister and missile nose and a fixed sensor array that will detect MMH and $NO_2$ at toxic (PEL) levels.

**Brief Description of the Research Carried Out:**

**Sensor Fabrication and Testing:** designed and fabricated MEMS chips with chemicapacitive, temperature and humidity sensors; fabricated a sensor array based on the chemicapacitive sensor systems for detection of hypergolic propellants; developed and test new coatings for target chemicals; characterized the coated sensors under simulated field conditions, varying temperature, humidity, and analyte concentrations.

**Hardware Systems Development**: redesigned motherboard to reduce power requirements and size; designed robust package(s) for new operation criteria.

**Software Systems Development:** develop algorithms for pattern recognition of hypergolic chemicals in the presence of interferrents

**Prototype Design:** based on the Phase I test results initiated the design of an inexpensive detector system that will meet all requirements for a hypergolic chemical detection system capable of being used after further development in Phase II.

**Research Findings/Results:**

**Sensor Fabrication and Testing**: Successfully synthesized and characterized against interferrents and rocket fuels: functionalized polysiloxanes (2), polycarbosilanes (3), and gold nanoparticles (5). Characterized commercial polymers (3) against interferrents and/or hypergolic compounds. Developed sensor arrays with proprietary and commercial chemoselective materials. Determined the change in capacitance of these arrays against interferrents (water, acetone, ethanol, octane) and hypergolic compounds ($NH_2NH_2$, $CH_3NHNH_2$, $(CH_3)_2NNH_2$, $NO_2$).

**Hardware Systems Development**: determined the temperature response of our MEMS chips; redesigned motherboard reduced power requirements by approximately 70%. Continued collaboration with Naval Research Laboratory into the utilization of a CASPAR preconcentrator. Began the research and development of a proprietary preconcentrator

**Software Systems Development**: began design a software algorithm capable of measuring outputs from the chemicapacitive sensors, temperature sensor, and humidity sensor; began initial testing of algorithm versus temperature and humidity variations; began testing of algorithm against interfering vapors; determined requirements for pattern recognition and Phase II development.

**Prototype Design**: Phase I prototype complete that would be capable of detection in simulated field conditions.

**Potential Applications:**

*Missile Defense Applicaiton*:

**KEI System:** Multi-tiered system capable of detecting in dynamic range from the LEL of fuels (MMH, Hz or UDMH ~10000 ppm) in the vehicle nose and canister to the PEL of fuels MMH (10 ppb) and oxidizers (NTO: PEL of $NO_2$ is 5 ppm) in the shipboard compartment.

*Other applications for a low-power accurate substituted and unsubstituted hydrazine sensor*:

**Rocketry**: hydrazines are extensively used as liquid fuels in launch vehicles. Sensor suite would quickly detect a catastrophic leak and would serve as a monitor for worker safety.

**Industry**: detection of hydrazines in an industrial environment for worker safety and to provide an alarm system for an explosive leak.

**Task 1. a. Sensor Fabrication and Testing:** Design and fabricate MEMS chips with chemicapacitive, temperature and motion sensors.

The temperature response of our sensors was determined by testing an on-chip resistive temperature device with a room temperature resistance of approximately 15000 to 17000 ohms and a sensitivity of 10 to 12 ohms per degree. An annealing procedure was applied to reduce high temperature drift (Figures 1 and 2).

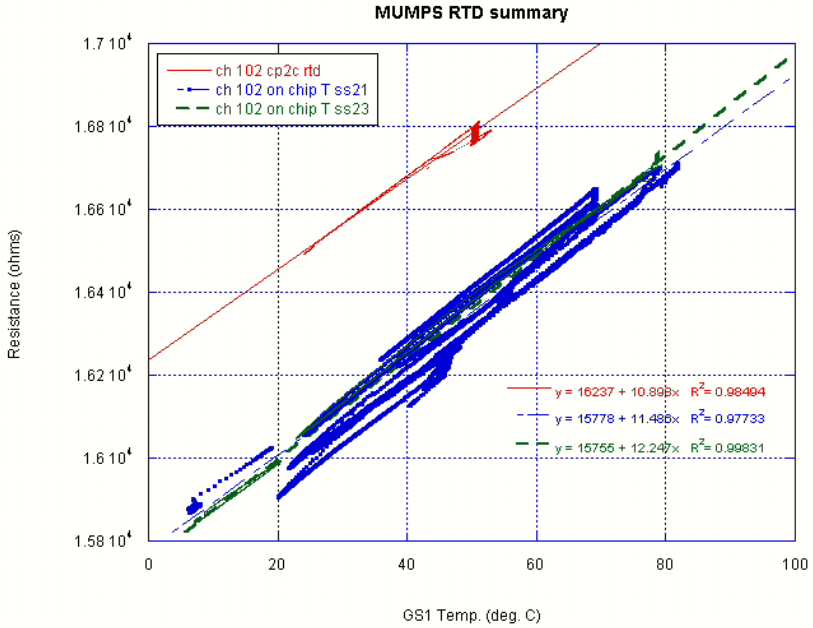


**Figure 1.** Resistance and Temperature Graph for the RTD on Three Different Sensor Chips.

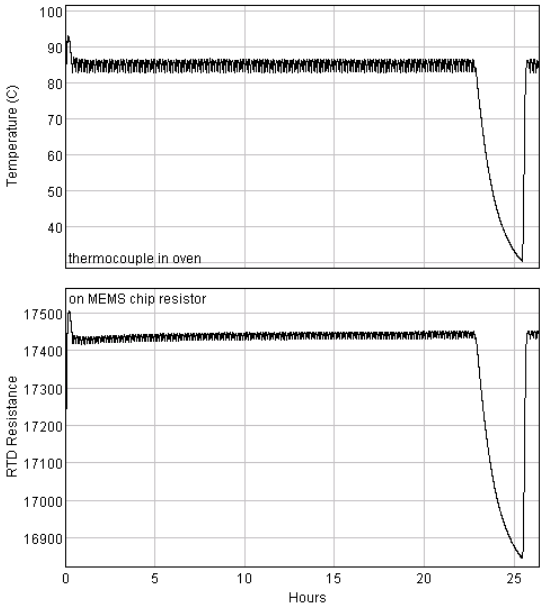


**Figure 2.** Resistance and Temperature Graph for the RTD after Anneal.

Changes are being made to the next generation of Seacoast's sensor readout circuits to use this RTD as the real-time temperature measurement. Testing of the new circuit is scheduled for late 2005.

**Task 1. b. Sensor Fabrication and Testing:** Fabricate a sensor array based on the chemicapacitive sensor systems for detection of hypergolic propellants.

In response to consultation with Mr. Benjamin Tritt, the response speed of a sensor array previously tested against interferrents was investigated. As a representative example, we have extracted the response speed of a functionalized polysiloxane (SXFA, ADIOL) and two functionalized hyperbranched polycarbosilanes (HC, NmA) (Figure 3).

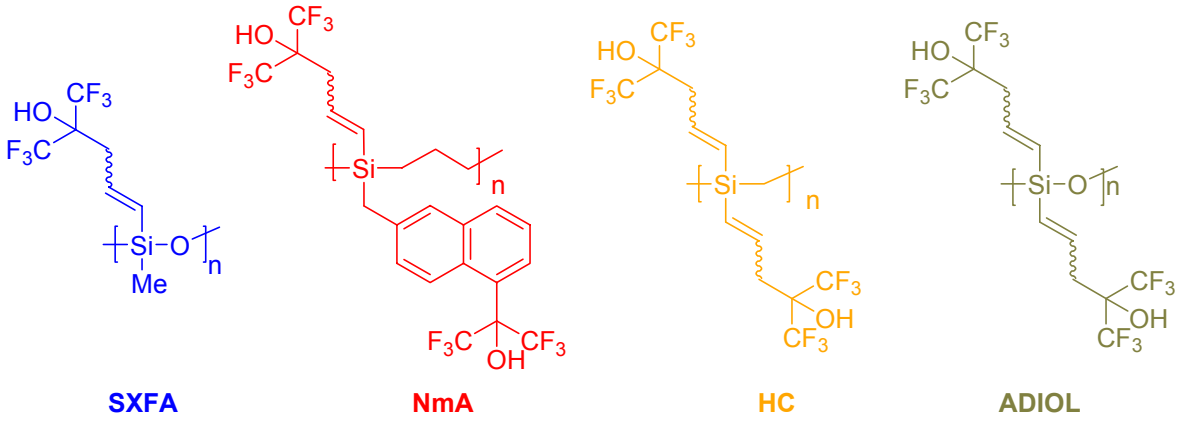


**Figure 3.** Representative Polymers Used for Speed of Response.

These polymers along with three others (PEI, PEO, PECH) were tested against the identified interferrents (acetone, ethanol, octane, and water) and these data were reported (*vide infra*). From these data we extracted the response speed (Figure 4)

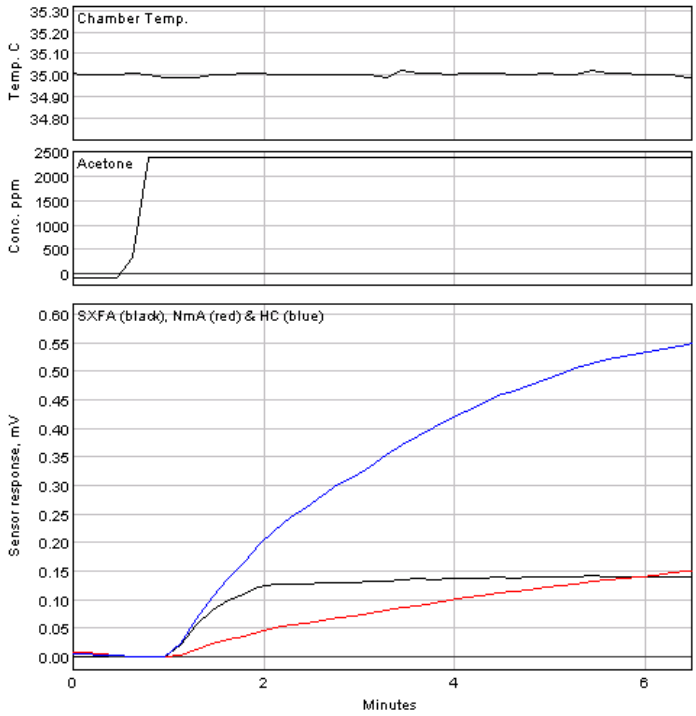


**Figure 4**. Response Speed of Three Polymers to Acetone (RH ~ 0%). Data is Baseline Corrected for Sensor Offset at 0 ppm Acetone. All Polymers Tested Simultaneously on the Same Chip.

The two figures of merit obtained from these data are:

- Onset time ($t_{onset}$): time at which the signal is >3x the baseline noise
- Equilibrium time ($t_{eq}$): time to reach 90% equilibrium response

For the onset time, both the HC and the SXFA are quite similar ($t_{onset} \approx 5$ seconds) whereas the NMA shows an offset time two to three times slower. For the equilibrium time, the functionalized polysiloxane, SXFA, has the shortest $t_{eq}$ of approximately 1 minute. The temperature dependence of the response speed of these polymers (cf Figure 3) was also determined (Figure 5)

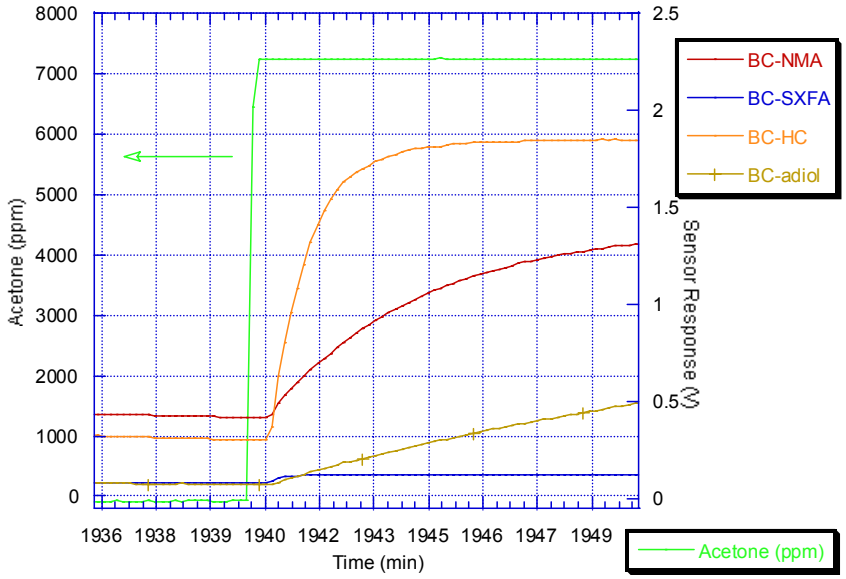


**Figure 5**. Response speed of four polymers to acetone (RH ~ 0%, T = 25º C).

The ~1.5 minute delay from the acetone pulse to the sensor response is from the void or dead volume in the system (the time from the detection of the acetone concentration at the mass flow controller to the responses in the sensor). The speed of response is also dependent upon the temperature of the test chamber (Figure 6).

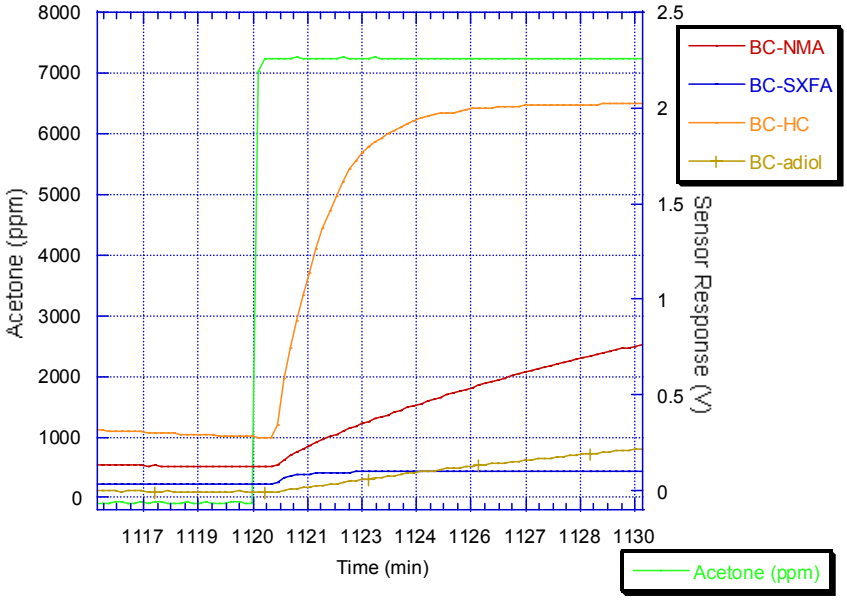


**Figure 6**. Response speed of four polymers to acetone (RH ~ 0%, T = 35º C).

For the onset time, both the HC and the SXFA are quite similar ($t_{onset} \approx 5$ seconds) whereas the NMA shows an offset time two to three times slower. For the equilibrium time, the functionalized polysiloxane, SXFA, has the shortest $t_{eq}$ of approximately 1 minute.

**Task 1c. Develop and test new coatings for target chemicals**

***Hybrid-Organic-Inorganic Materials:*** Initial experiments into the synthesis of selective materials began using α,ω-bis(triethoxysilyl) monomers with aqueous PEI as catalysts (Scheme 1).

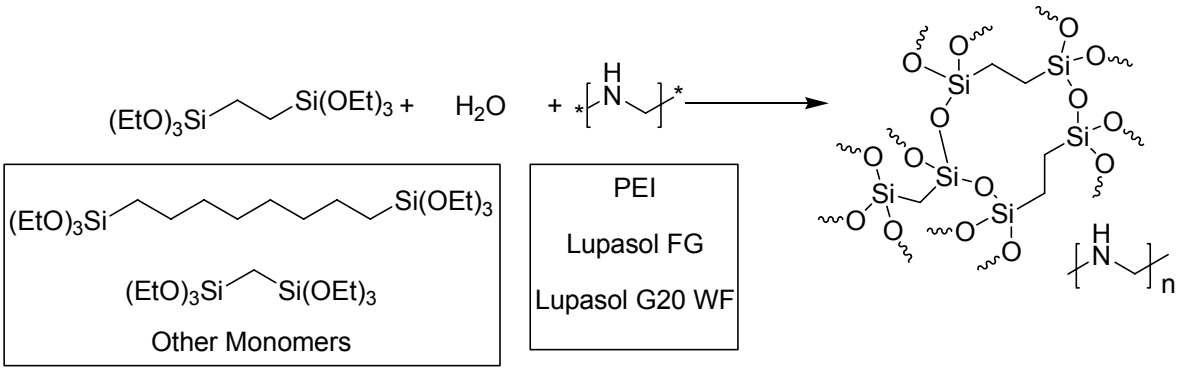


**Scheme 1**. Synthesis of Hybrid Materials for Potential Sensing of Hypergolic Compounds.

The ethylene and methylene bridged materials resulted in white precipitate and the octyl bridged materials failed to gel. Both results prompted a move to other chemoselective materials. Next, the use of a multilevel composite material for the detection of hypergolic compounds was completed (Figure 7).

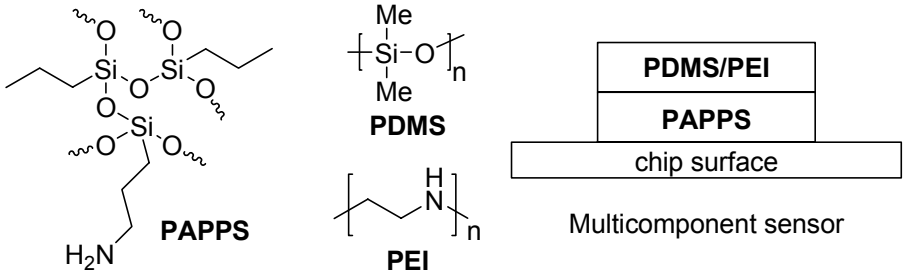


**Figure 7.** Architecture of Multi-level Sensor.

***Functionalized Gold Nanoparticles*** Previously reported results using alkyl thiol stabilized gold nanoparticles[1] in mass-based sensors encouraged us to further explore functionalized gold nanoparticles (d~1.5 nm). Accordingly, their syntheses were expanded to included different terminal functional groups. (Scheme 2).[2]

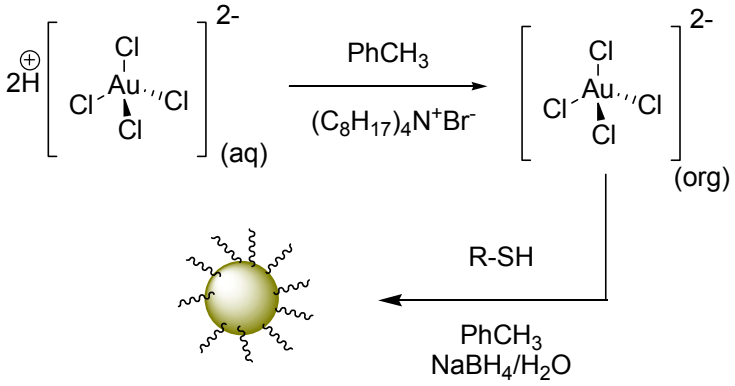


| R Group | Name |
|---|---|
| (n-$C_7H_{15}$) | Au-C7-H |
| (n-$C_{12}H_{25}$) | Au-C12-H[3a] |
| 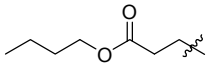 | Au-C2-*n*-BuEster |
| HO(n-$C_6H_{12}$) | Au-C6-OH[4] |
| HOOC(n-$C_{11}H_{22}$) | Au-C11-COOH[2] |

**Scheme 2**. Synthesis of Thiol-coated Functionalized Nanoparticle Gold for Sensing of Hypergolic Compounds

Adapting a 2-phase synthetic scheme using tetra-*n*-octyl ammonium bromide as the phase transfer catalyst and sodium borohydride as the reducing agent, we synthesized 5 functionalized nanoparticulate gold materials. We have previously shown that gold nanoparticles functionalized with $C_6$ and $C_8$ thiols are exceptionally sensitive to aromatic and aliphatic organic compounds.[5] These compounds were coated onto a sensor chip and were tested against the interferrents and the hypergolic compounds.

***Functionalized Polycarbosilanes and Polysiloxanes***. The sensing properties of linear and hyperbranched polycarbosilanes and polysiloxanes have been well estabilished.[6] The synthesis of the both classes of compounds consists of an initial polymerization followed functionalization of the alkene using hexafluoroacetone. Thus, a hyperbranched poly(methylsilane) designated HC was synthesized by the Grignard initiated polymerization of chloromethyltrichlorosilane,[7] condensation of allyl magnesium bromide with the residual chlorosilane moeities, and post-polymerization functionalization with hexafluoroacetone.[8] (Scheme 3).

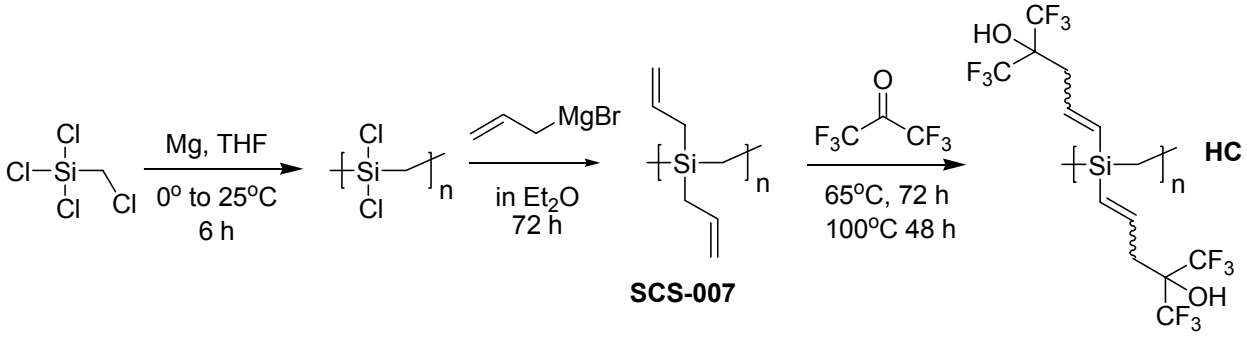


**Scheme 3.** Synthesis of Hyperbranced Polycarbosilane

This material was prepared in acceptable yield (25-75%) and displayed differential sensitivity to analytes and interferents (*vide infra*). The hyperbranched precursor polymer was also used as the starting materials for novel tetra-ol polymer (Scheme 4).

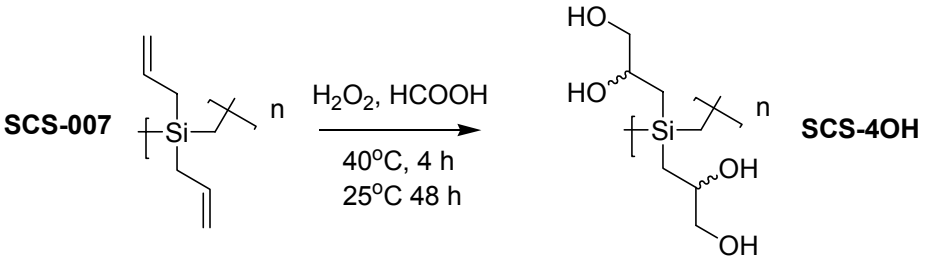


**Scheme 4**. Dihydroxylation of Diallylpoly(methyl)carbosilane)

Using a standard oxidation method[9] SCS-4OH was prepared in moderate yield (25%). Upon work-up, the polymer changed from a viscous liquid to a light tan solid.

In contrast, functionalized linear polysiloxanes were prepared from commercially available polymers (i. e. silicones) or were synthesized by the polycondensation of substituted dichlorosilanes followed by postpolymerization functionalization with HFA.[8] Thus, starting with a commercially available polysiloxanes, we prepared a multifunctional material using aluminum trichloride as the alkylation catalyst (Scheme 5)[7e]

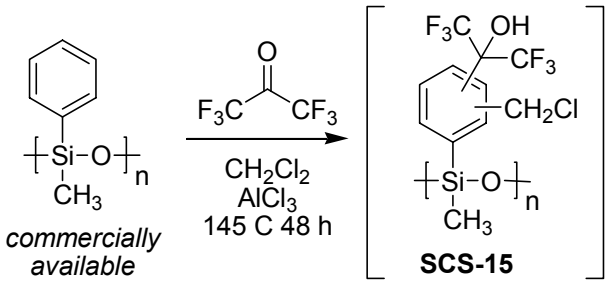


**Scheme 5.** Synthesis of Functionalized Polysiloxane.

The synthesis of a polysiloxane analogue to HC was also attempted by the condensation of allyl magnesium bromide with allyltrichlorosilane followed by polycondensation and functionalization (Scheme 6).[7e]

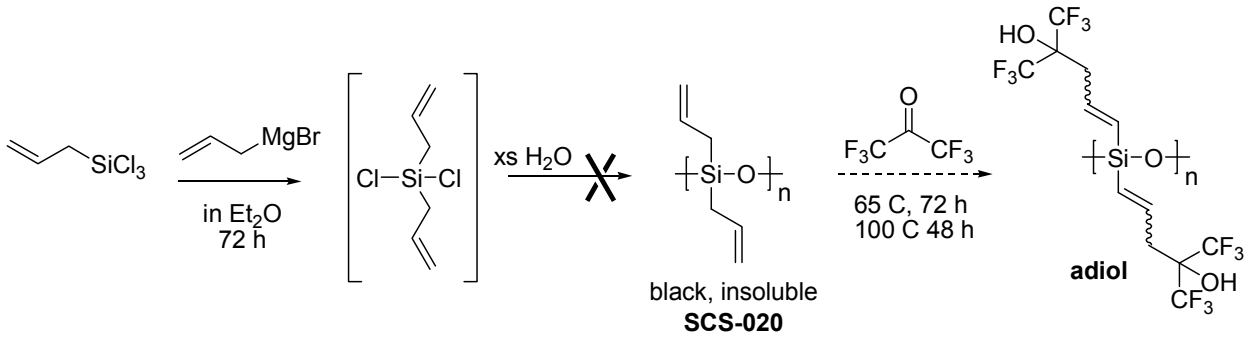


**Scheme 6**. Attempted Synthesis of Polysiloxane Derivative of HC.

The poor results in the polymerization of dichloro-dialyllsilane to give polysiloxane (SCS-020) may be due to incomplete reaction of the Grignard reagent with allyl-trichlorosilane. During the subsequent hydrolysis and condensation, the resultant trifunctional silicon ($RSiCl_3$ or $T^30$)[10] may act as a crosslinking agent resulting in the observed low solubility. In contrast, the commercially available allyl-methyl dichlorosilane smoothly polymerized to give polysiloxane **SCS 24** in quantitative yield. Functionalization with hexafluoroacetone in chloroform gave SXFA in quantitative yield (Scheme 7).

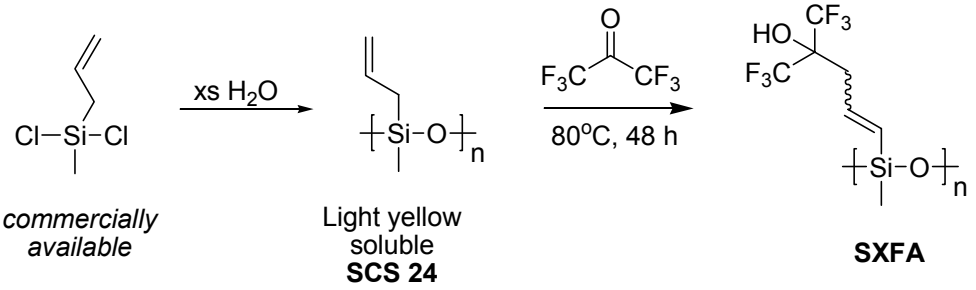


**Scheme 7**. Synthesis of SXFA

All the polycarbosilanes and polysiloxanes were tested either against the hypergolic fuels, oxidizers, interferrents, or both.

The final class of compounds investigated was metal centered phthalocyanines variably substituted with *tert*-butyl groups to prevent crystallization and allow thin film formation (Figure 8)

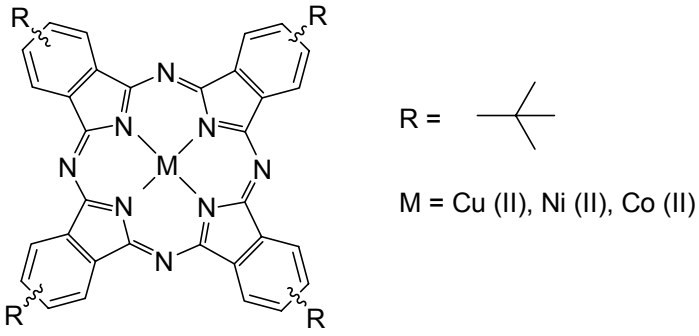


**Figure 8.** Metal Centered Phthalocyanines tested against interferrents and $NO_2$

These materials were prepared in the laboratory of Professor William Trogler (UCSD) and similar compounds have previously shown sensitivity to organophosphonates (DIMP) and NO.[11]

**Task 1d characterized the coated sensors under simulated field conditions, varying temperature, humidity, and analyte concentrations**

A new chemically inert test system was designed and a chemically inert (PEEK) test chamber was completed. Initial testing involved the examination of both commercially available materials and novel materials against previously identified interferrents (Table 1).

**Table 1.** Polymers Proposed for Detection of Fuels, Oxidizers, and Interferrents.

| Agent Class | Chemical | Candidate Polymers |
|---|---|---|
| **Fuels** | Hydrazine | Siloxane fluoroalcohol (SXFA), Polyethyleneimine (PEI) |
| | Monomethyl Hydrazine | HC, NMA<br>Poly(cyanopropyl siloxane) (OV-275) |
| | Dimethyl Hydrazine | Siloxane fluorodiol (Adiol) |
| **Oxidizers** | RFNA | SXFA, PEI |
| | MON-25 | Polyamines and Polycarbonyls |
| **Interferents** | Ethanol | SXFA |
| | Acetone | PEO |
| | Octane | Poly(ethylene-co-vinyl acetate) (PEVA), Polyisobutylene |
| | Humidity | Poly(aminopropyl propyl siloxane) (PAPPS) |

Polyethylenimine (obtained from Sigma Aldrich Corporation, Catalog # 40,872-7 Polyethylenimine, $M_w$ ~ 25,000), a hydrophilic branched cationic polymer $(CH_2CH_2NH)_n$, was tested against the interferents but only displayed a significant response to water (Figure 9).

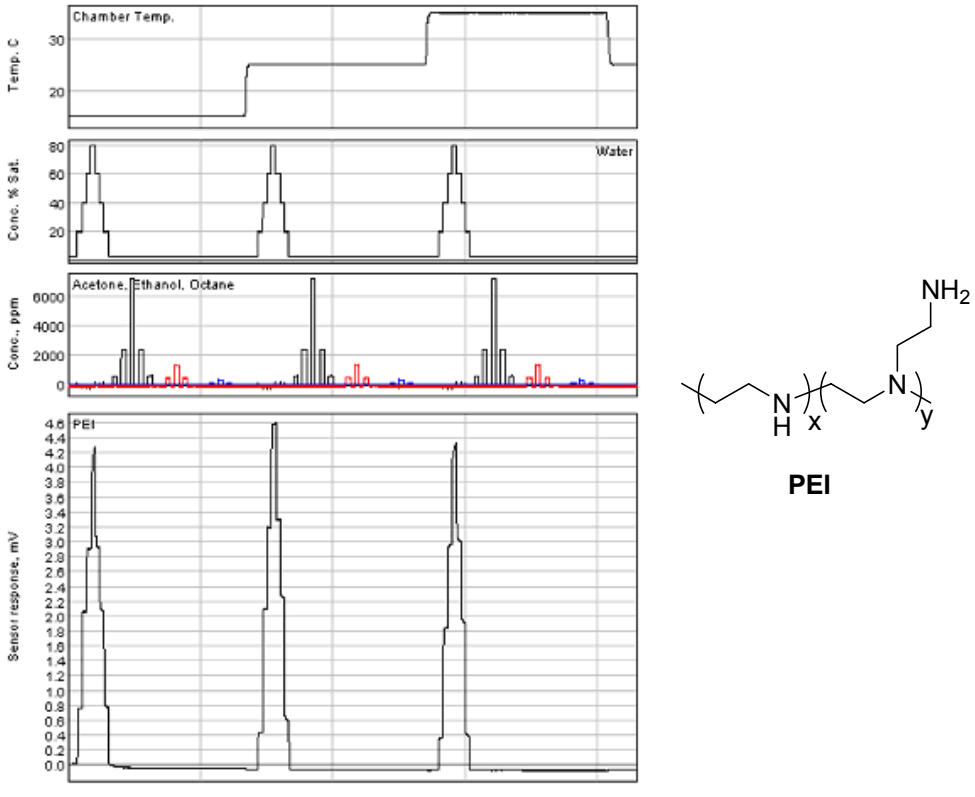


**Figure 9**. Response of PEI to Interferents.

We continued the interferrent tests against additional polymers (Figure 10) under variable humidity and temperature (Figure 11) and under low humidity at ambient temperature (Figure 12).

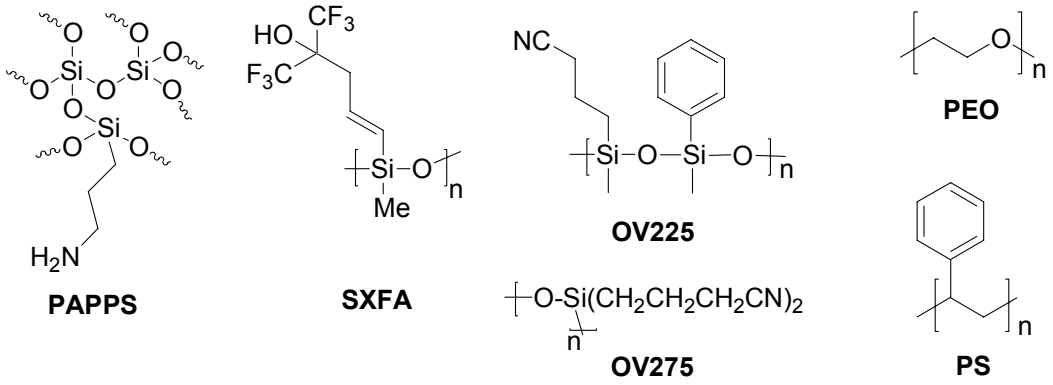


**Figure 10.** First Set of Polymers Tested Against Interferents.

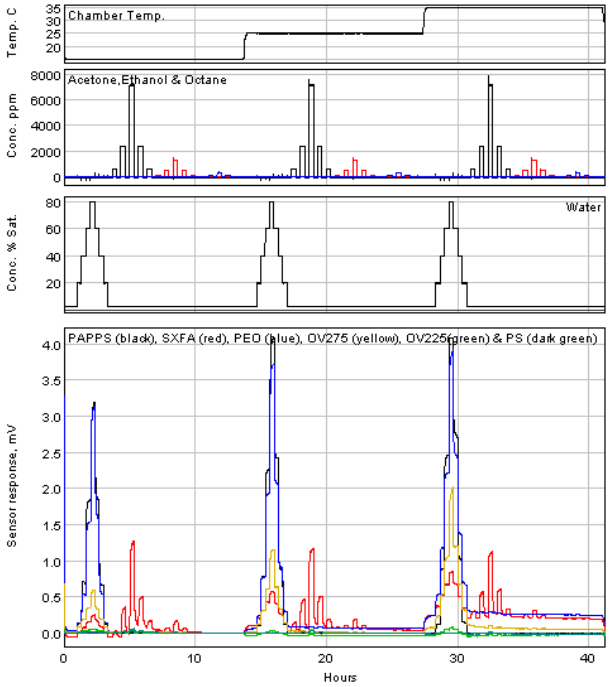


**Figure 11**. Test of Chemoselective Polymers Against Interferents with Variable Temperature and Humidity. Key: PAPPS: blue; SXFA: red, OV275: yellow; OV225: green; PS: dark green.

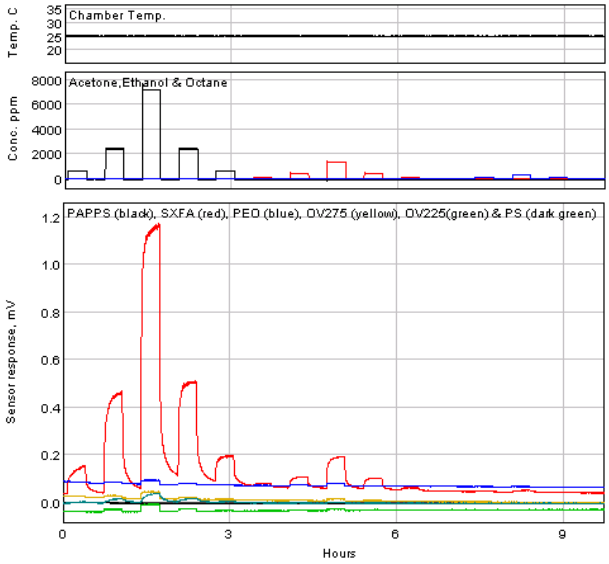


**Figure 12.** Test of Chemoselective Polymers Against Interferents with Low and Ambient Temperature. Key: PAPPS: blue; SXFA: red, OV275: yellow; OV225: green; PS: dark green

In the initial array of materials (*vide supra*), the hydrophilic polymers (PAPPS, PEO) showed strong responses to humidity regardless of the chamber temperature whereas the functionalized polysiloxanes (OV275, SXFA) showed a temperature dependent response to water vapor. Of the polymers tested in the first array, only SXFA showed a measurable response to acetone and ethanol. The second series of polymers consisted of functionalized polysiloxanes (cf Figure 3), and organic (co) polymers (PEI, polyethylene co polyvinylacetate (PEVA). These tests were performed under variable humidity and temperature (Figure 13) and under low humidity at ambient temperature (Figure 14).

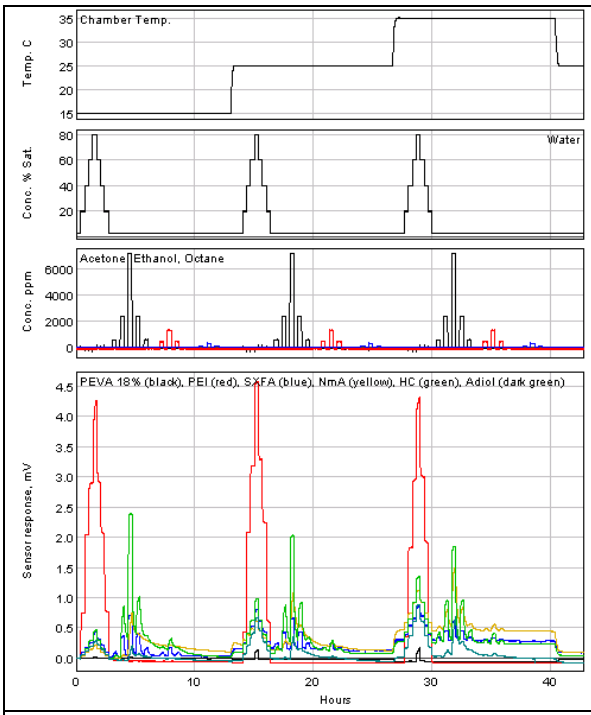


**Figure 13**. Test of Chemoselective Polymers Against Interferents with Variable Temperature and Humidity. Key: PEVA black; PEI red; SXFA blue; NmA yellow; HC green; ADIOL dark green

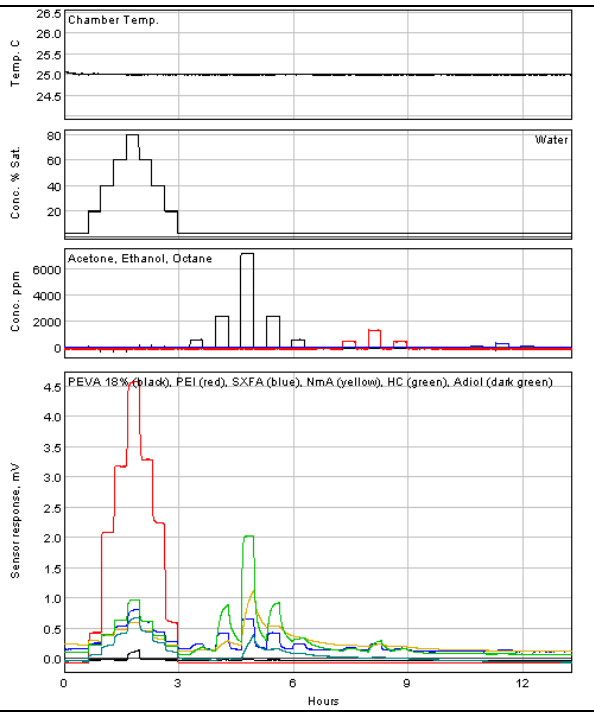


**Figure 14**. Test of Chemoselective Polymers Against Interferents with Low and Ambient Temperature. Key: PEVA black; PEI red; SXFA blue; NmA yellow; HC green; ADIOL dark green

A similar trend was observed in the second array of materials: PEVA showed the strong temperature-independent response to water vapor whereas the other polymers showed an increasing response to water vapor with increasing chamber temperature. A differential response to polar protic and polar aprotic organic compounds was observed with the functionalized polysiloxane (SXFA) and polycarbosilane (HC). None of the materials tested showed a significant response to octane. Both the functionalized carbosilane (SCS15) and the functionalized polysiloxane (SCS 20) displayed a strong response to water and a weak responses to acetone (Figure 15).

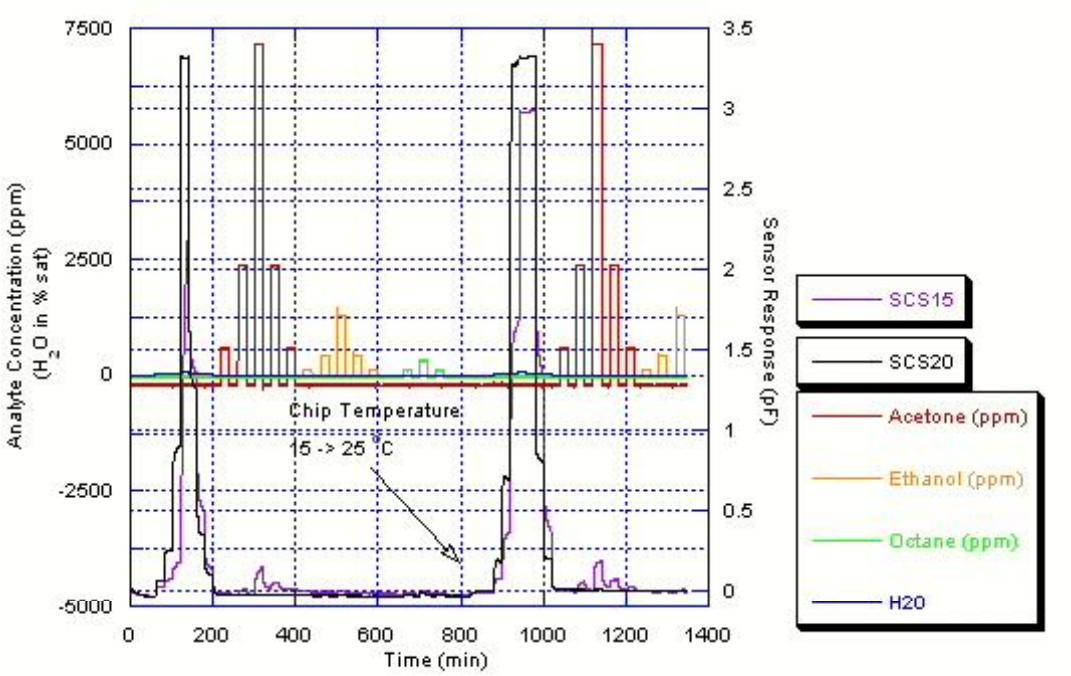


**Figure 15**. Response of SCS 15 and SCS 20 to Interferrents

Testing of the functionalized gold nanoparticles showed that whereas the carboxylic acid and alkanol functionalized materials showed a significant response only to water, the Au:C7 material displayed a response to the other interferrents including octane although it retained water sensitivity (Figure 16).

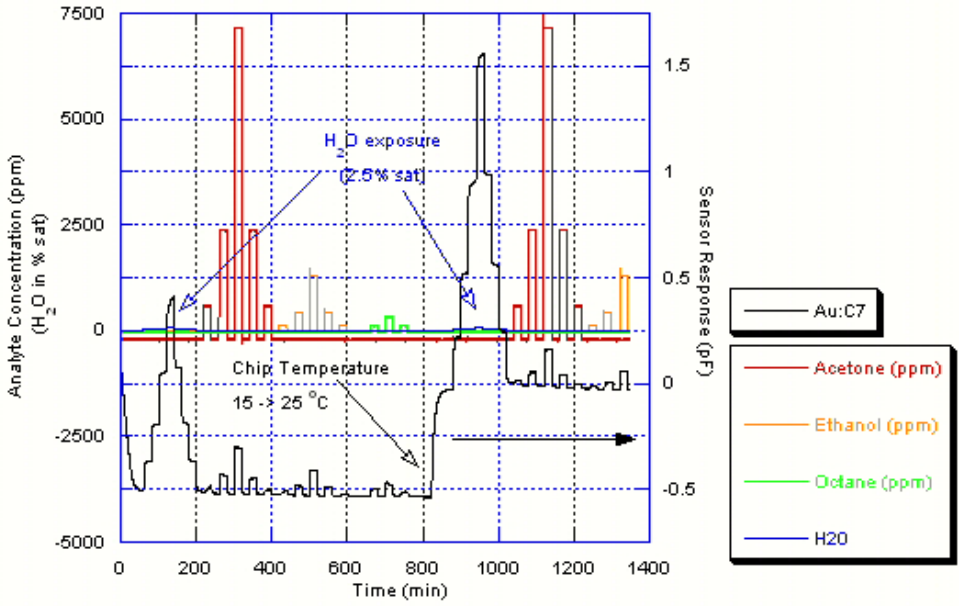


**Figure 16**. Response of **Au:C7** to Standard Interferrents

The *n*-butyl ester functionalized gold nanoparticle (Au:C2:*n*Bu-Ester) also showed excellent response to the interferrents with lower water sensitivity (Figure 17).

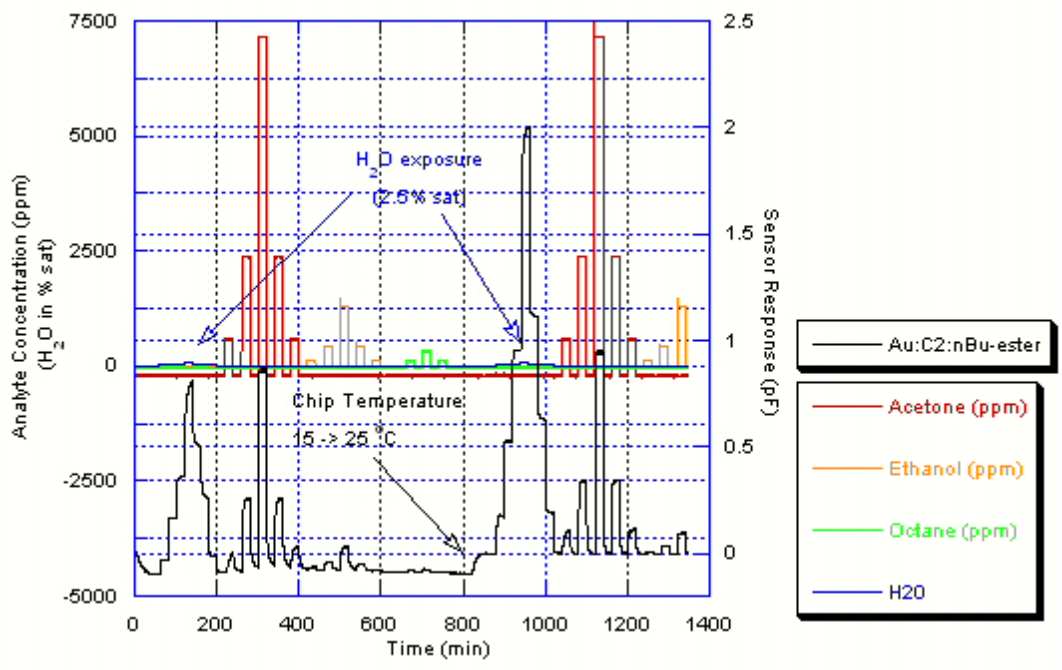


**Figure 17**. Response of **Au-C2-*n*BuEster** to standard interferrents

In contrast to the water sensitivity of the gold nanoparticles, the metal centered phthalocyanines only showed a small response to high concentrations of water, acetone and ethanol (Figure 18)

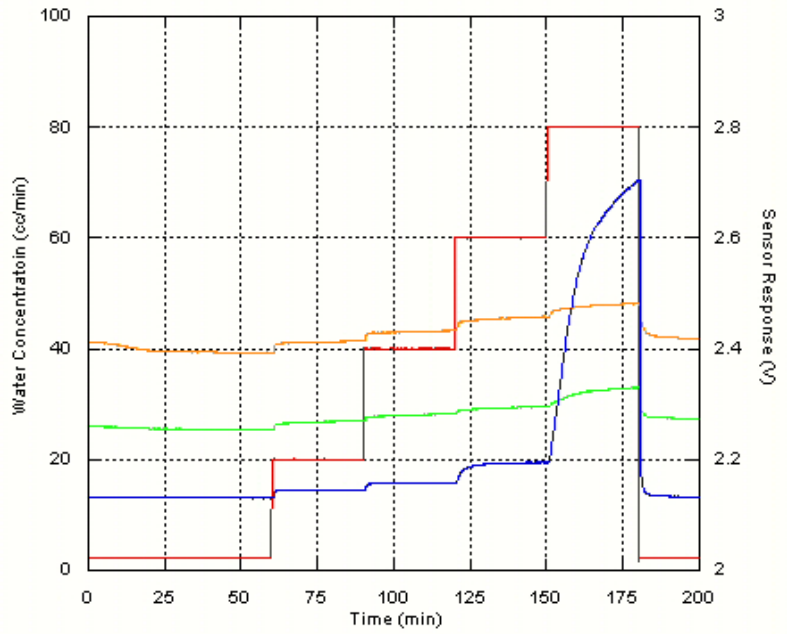


**Figure 18.** Response of Metal Centered Phthalocyanines to water. Key: water: red; Co(II) phthalocyanine: orange; Ni(II) phthalocyanine: green; Cu(II) phthalocyanine: blue

The relative sensitivity of these polymers and network materials to the interferents guided the eventual design of the sensor chip that will "filter" out noise and identify the fuel and oxidizers in a complex environment (Table 2).

**Table 2**. Polymer Structure and Chemical Selectivity

| Name | Structure | Chemical Selectivity | Name | Structure | Chemical Selectivity |
|---|---|---|---|---|---|
| **PEO** | 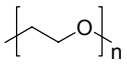 | $H_2O$ (T independent) | **PEVA** | 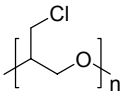 | $H_2O$ (T dependent) |
| **OV275** | 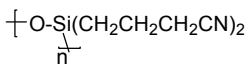 | $H_2O$ (T dependent) | **PEI** | 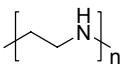 | $H_2O$ (T independent) |
| **PAPPS (see Figure 7)** | 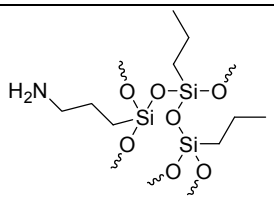 | $H_2O$ (T independent) | **SXFA** | 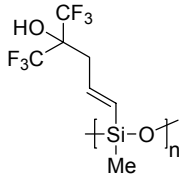 | $H_2O$ (T dependent) |
| **NmA** | 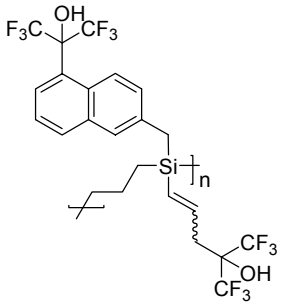 | $H_2O$ (T dependent) Acetone EtOH (T dependent) | **HC** | 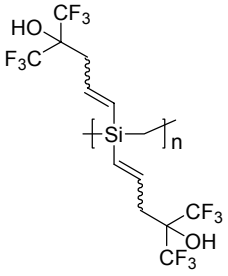 | $H_2O$ (T dependent) Acetone EtOH (T dependent) |
| **Adiol** | 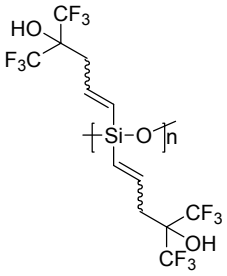 | $H_2O$ (T dependent) Acetone EtOH (T dependent) | **SCS-007** | 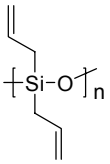 | Octane |
| | 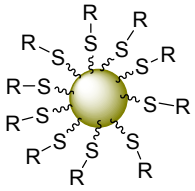 **R** | | **SCS-15** | 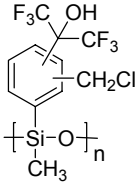 | $H_2O$, Acetone |
| **Au-C7-H** | ($n$-$C_7H_{15}$) | $H_2O$, acetone, EtOH | **SCS-4OH** | 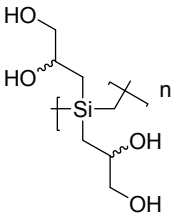 | $H_2O$, octane |
| **Au-C2-nBuEster** | 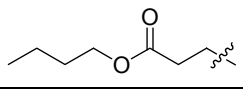 | $H_2O$, acetone EtOH | | | |
| **Au-C6-OH**[12] | ($n$-$C_6H_{12}$) OH | $H_2O$ | | | |
| **Au-C11-COOH**[11] | ($n$-$C_{11}H_{22}$) COOH | $H_2O$ | | | |
| **Cu(II)*t*BuPc** | *see Figure 6 | $H_2O$ | **Ni(II)*t*BuPc** | *see Figure 6 | EtOH, acetone |
| **Co(II)*t*BuPc** | | EtOH acetone, | | | |

We also began characterizing the response of our sensors to the hypergolic compounds. Using the-interferrent data gathered (cf Table 2) the following polymers were selected for the detection of hydrazine, MMH and UDMH (Figure 19)

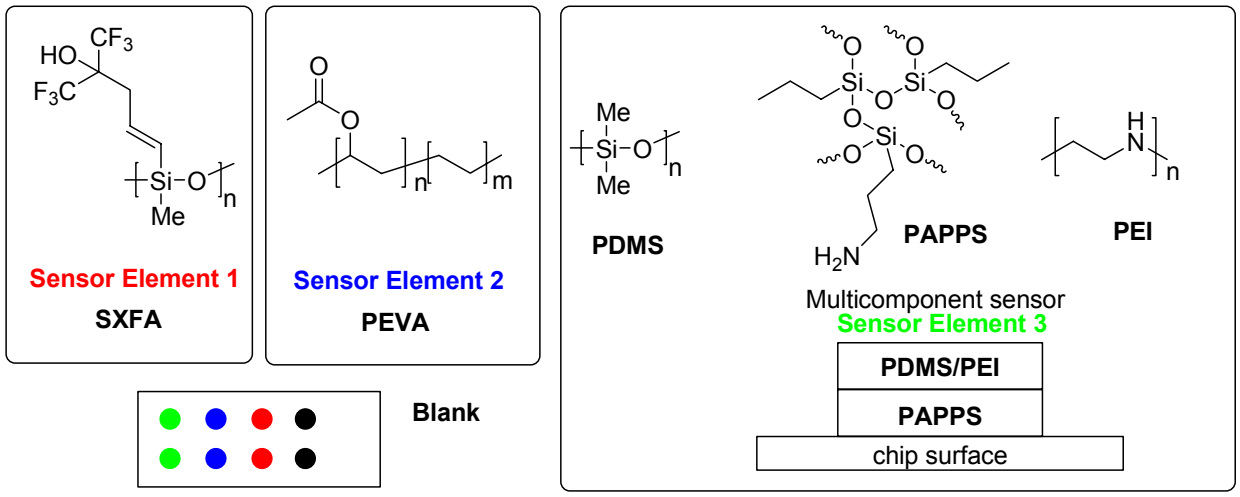


**Figure 19.** Chemoselective materials used for the detection of MMH and UDMH.

We chose a range of materials including a fluorinated polysiloxane (SXFA), a commodity organic co-polymer (PEVA), and a proprietary mutlicomponent sensor consisting of a polysilsesquioxane core coated with a PDMS/PEI polymer blend. These materials were coated onto Seacoast Science's fixed plate capacitor sensor chip and either the voltage or capacitance was measured using previously developed boards. For hydrazine we conducted a series of experiments to examine the following variables:

- Relative Humidity
- Hydrazine concentration
- Chamber temperature
- Concentration gradient

At low relative humidity (nominal 0% RH) at 20ºC the sensors showed a significant response to moderate levels of hydrazine with a high noise level (Figure 20)

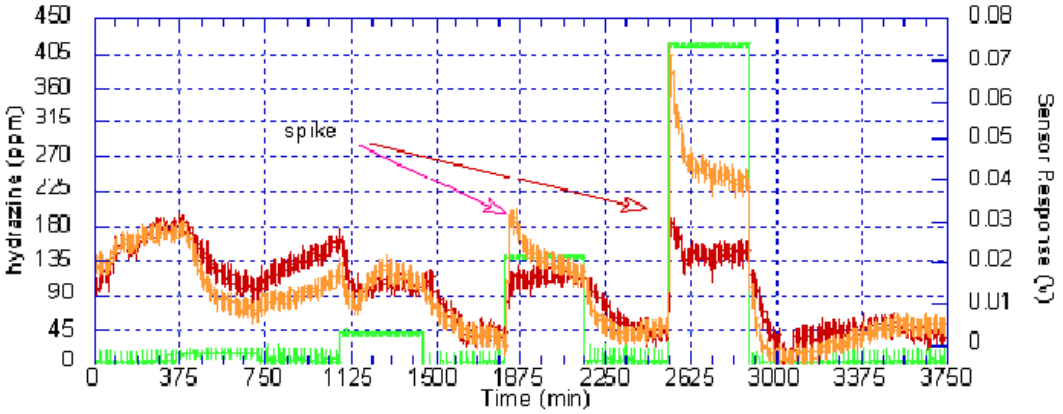


**Figure 20**. Initial Test of Sensors with Moderate Levels of Hydrazine Vapor (RH = 0%, T = 20ºC). Key: hydrazine: green; PDMS:PEI:PAPPS (see Figure 7): red; SXFA: orange

Despite the unstable baseline and the 'spikes' at the beginning of each increase in the hydrazine concentration, we were able to detect hydrazine at 135 ppm. We hypothesized that the rolling baseline and the 'spikes' were due to adventitious water in the hydrazine. We next tested the sensor at 50 % relative humidity (Figure 21)

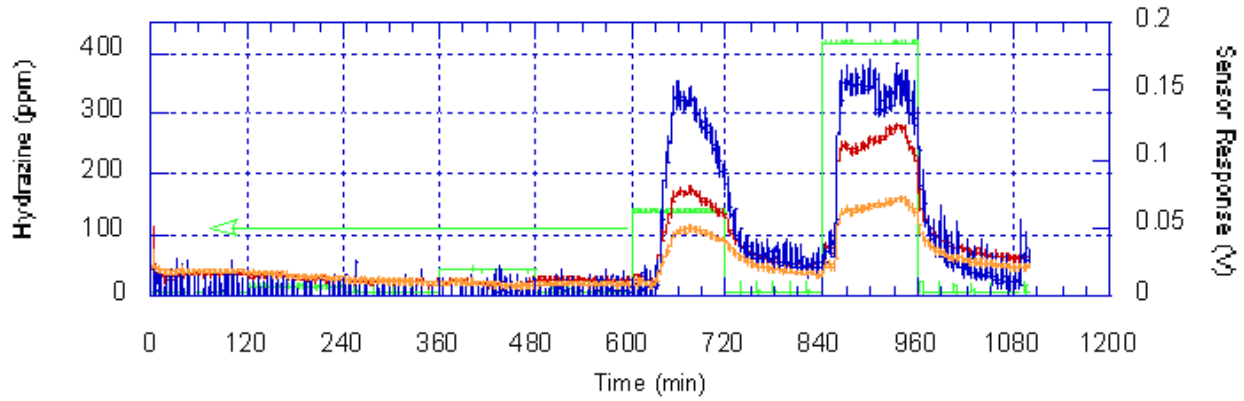


**Figure 21.** Sensor Response with Increasing Moderate Levels of Hydrazine Vapor (RH = 50%, T = 20ºC). Key: hydrazine: green; PDMS:PEI:PAPPS: red; PEVA; blue SXFA: orange

Although the spikes present at initiation of hydrazine exposure disappeared, the slow recovery of the sensor after the removal of the hydrazine vapor was troubling. One possible reason for this observation is an interaction between the hydrazine and the PFA tubing. To test this hypothesis, we examined the sensor response with decreasing concentration of hydrazine that would presumably 'passivate' the system surface (Figure 22).

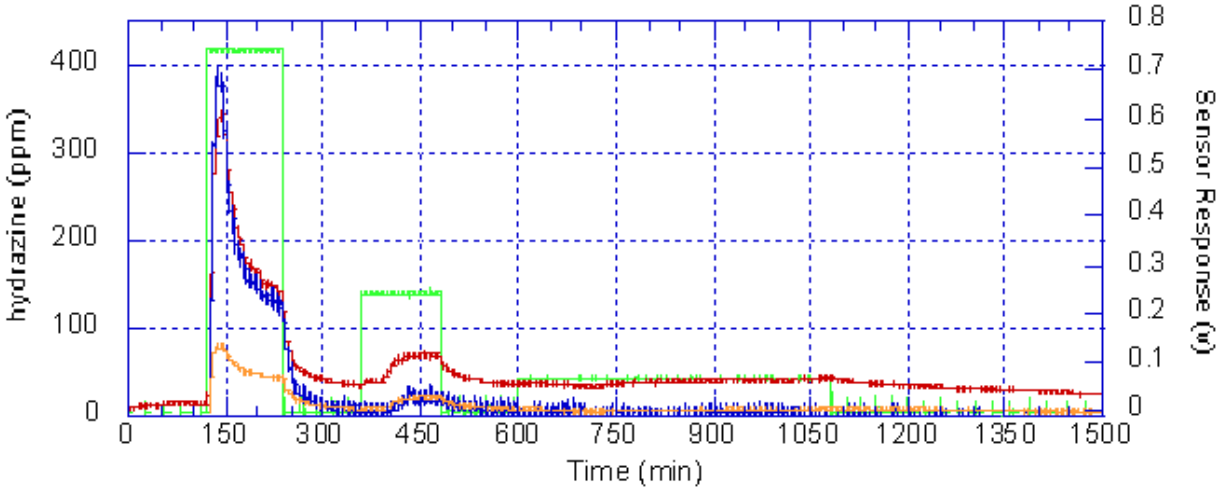


**Figure 22**. Sensor Response to Decreasing Concentrations of Hydrazine (RH = 50 %, T = 20ºC) Key: hydrazine: green; PDMS:PEI:PAPPS red; PEVA; blue SXFA: orange

This inversion of the concentrations allows the sensors to recover more rapidly at the terminus of the hydrazine vapor exposure. The initial spike followed by decay may be indicative of physical or chemical interaction between the hydrazine and the sensor itself (Scheme 8)

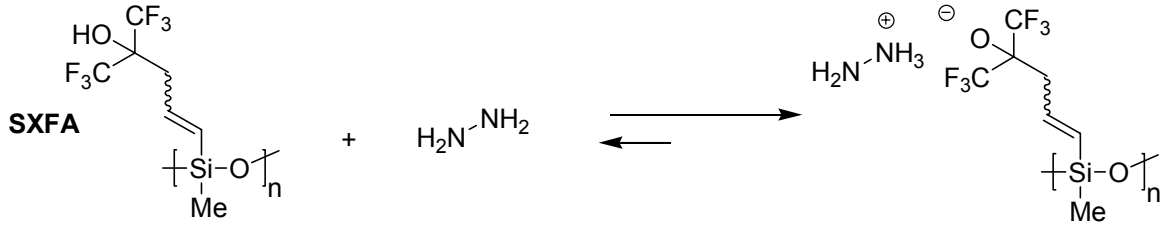


**Scheme 8.** Possible interaction between hydrazine and SXFA

At first glance, this proton transfer is thermodynamically disfavored with the $pK_a$ of perfluoroisopropanol ~18 and the $pK_a$ of the hydrazinium ion ~ 8 (see F. G. Bordwell *Acc. Chem. Res.* **1988**, *21*, 456, 463). However, since the

hydrazine is in the gas phase, the equilibrium may be forced to the right from the physical removal of hydrazine from the vapor stream. Another explanation is that the initial spike is from a pressure build-up that results as the hydrazine vapor is delivered to the sensor. Regardless of the explanation, the spike was absent at the exposure of the sensor to a lower concentration of analyte.

The final variable that we examined was the influence of the chamber temperature on the sensor response (Figure 23)

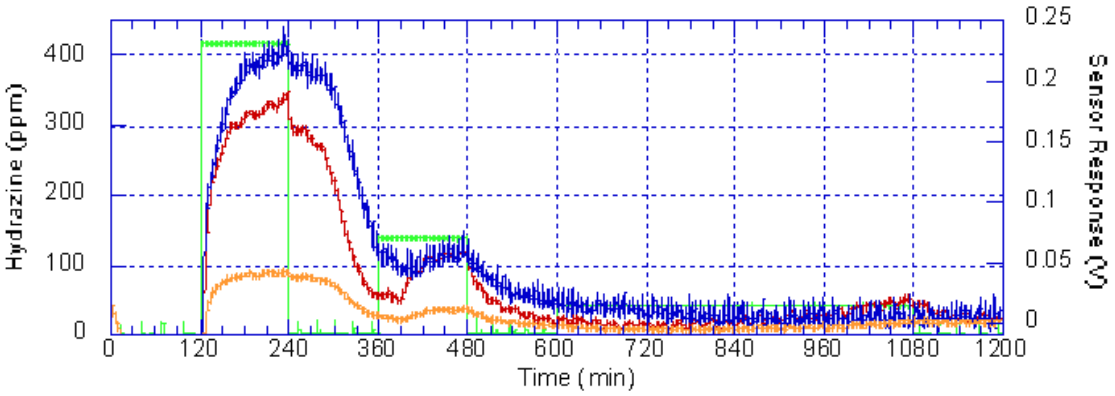


**Figure 23.** Sensor Response to Hydrazine (50% RH, T = 10ºC) Key: hydrazine: green; PDMS:PEI:PAPPS: red; PEVA; blue SXFA: orange

At the lower chamber temperature (**10ºC)** the initial spike of sensor response is absent, although the sensor recovery time is greatly extended. The magnitude of the sensor response is comparable to tests run at 20ºC. From the above graphs, we determined a limit of detection of 16.3 ppm using the multilevel sensor (PEI:PDMS:PAPPS).[13]

Our initial experiment showed that PEI/PDMS/PAPPS materials was most responsive to MMH (Figure 24)

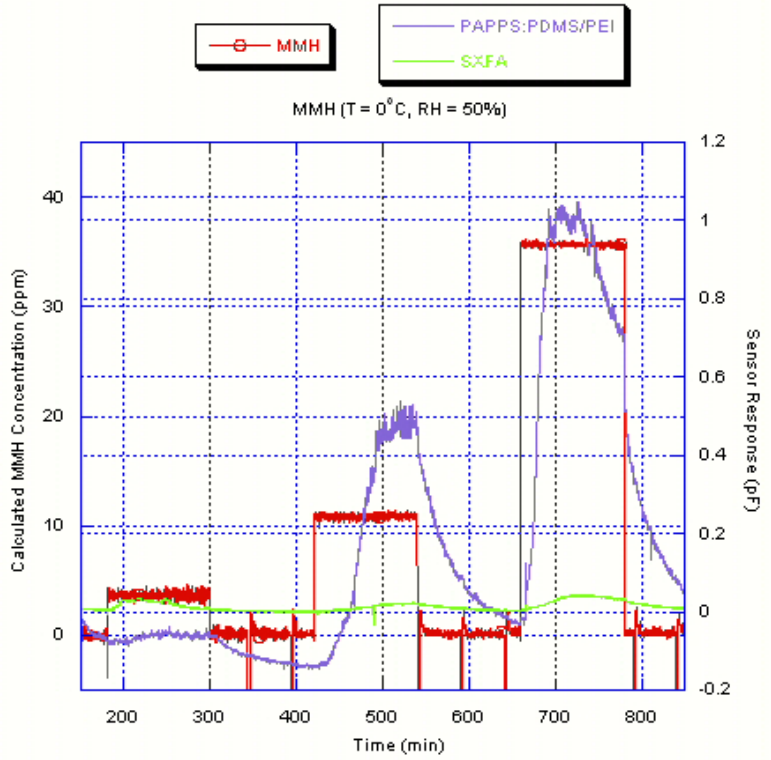


**Figure 24**. Sensor Response to MMH (RH ~ 50%, T = 0º C).

Note that the PECH data is not shown because it was completely unresponsive to MMH. We next examined the same sensor array with a low level exposure of MMH (Figure 25).

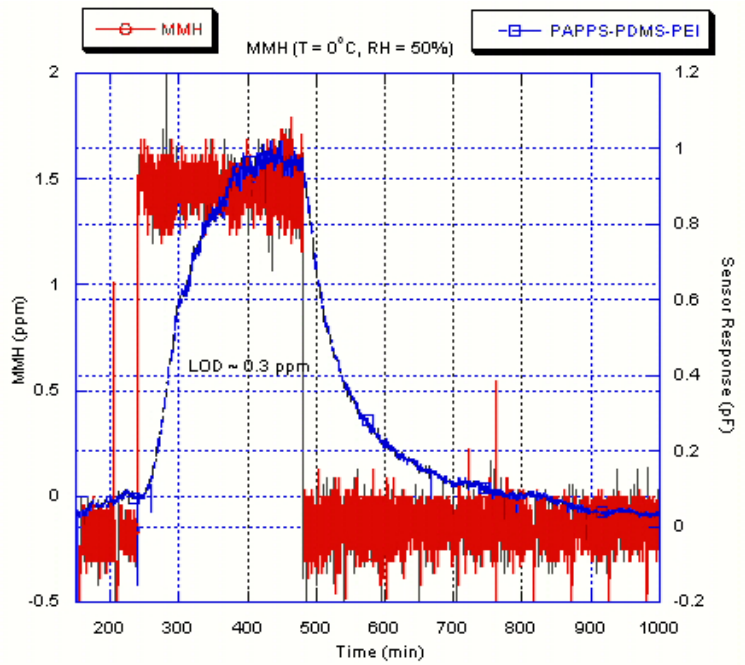


**Figure 25**. Sensor Response of PAPPS:PEI/PDMS to ~1.5 ppm concentration of MMH (RH ~50%, T = 0º C). Not only did this allow us to determine the limit of detection (~0.3 ppm) for MMH with the PAPPS:PEI/PDMS sensor, it also demonstrated the reversible nature of the MHH adsorption on the sensor surface. We next examined the effect of the relative humidity (RH) level to the sensor response in the presence of MMH (Figure 26)

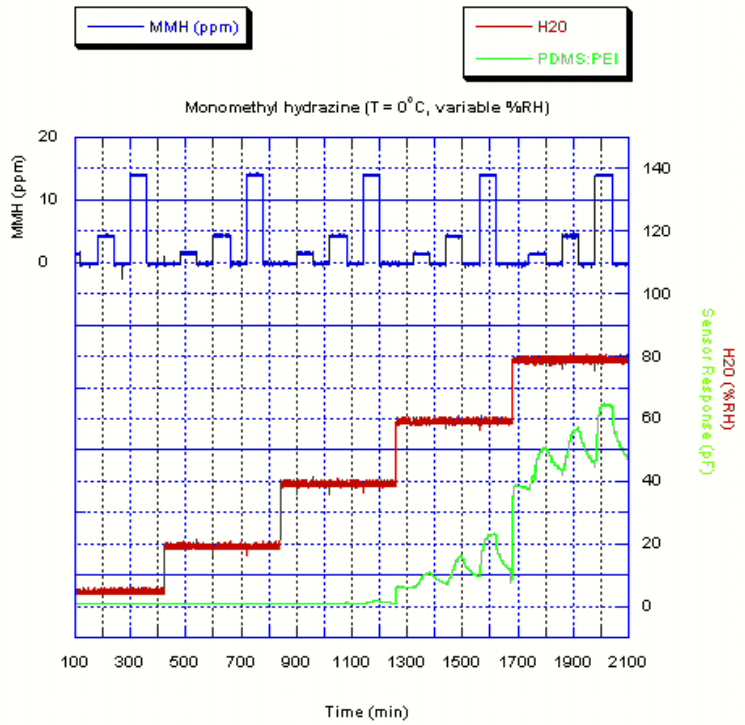


**Figure 26**. MMH/Humidity effects upon PAPPS: PEI/PDMS sensor

There appears to be a threshold of ~50% relative humidity that is necessary for the detection of MMH with the composite sensor. This threshold effect is more starkly illustrated by examining the sensor response at 0 and 50% RH (Figure 27).

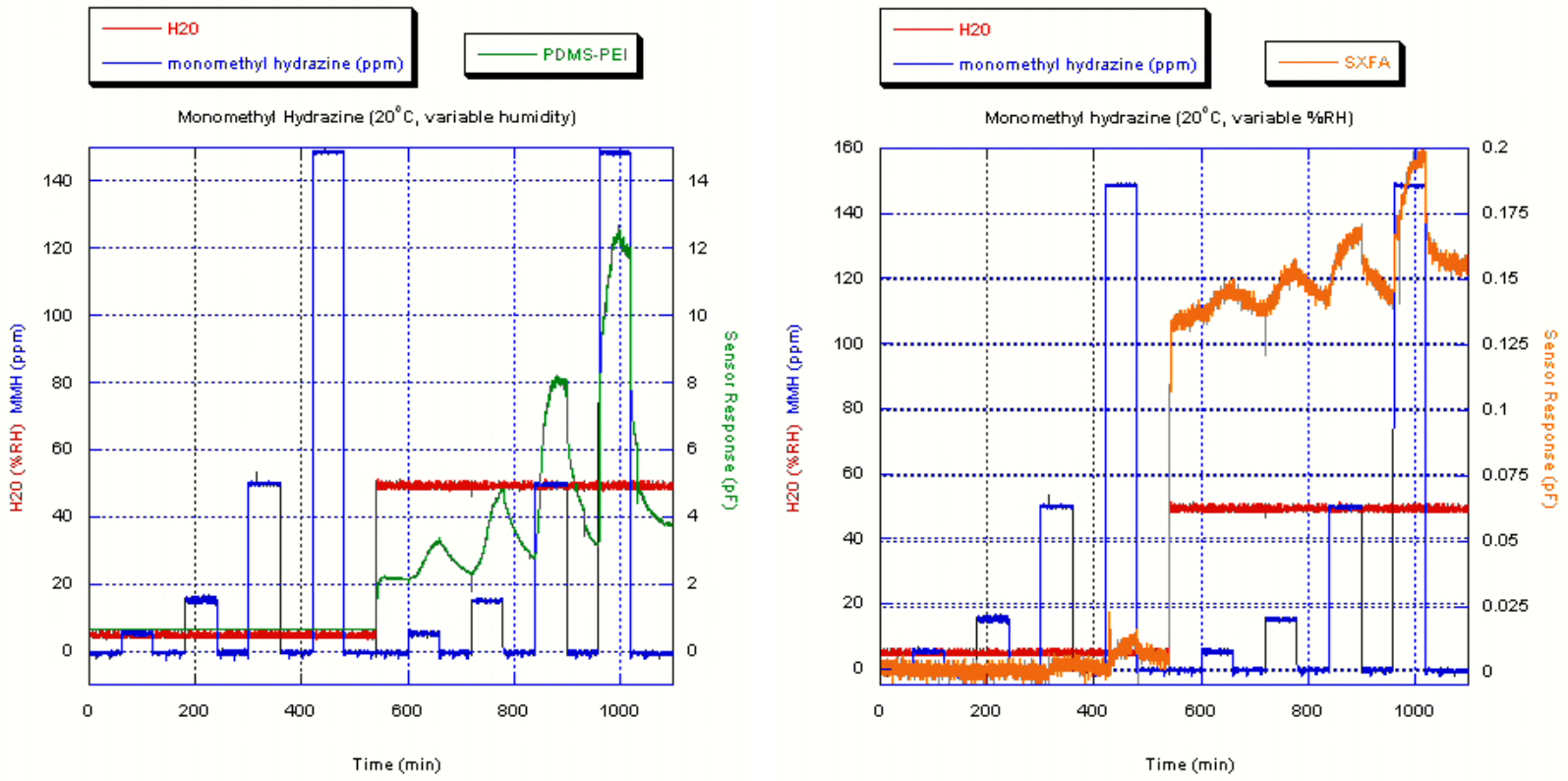


**Figure 27**. Sensor Response to MMH at 0 and 50% RH.

As similar sensor response pattern was noted for the detection of UDMH (Figure 28).

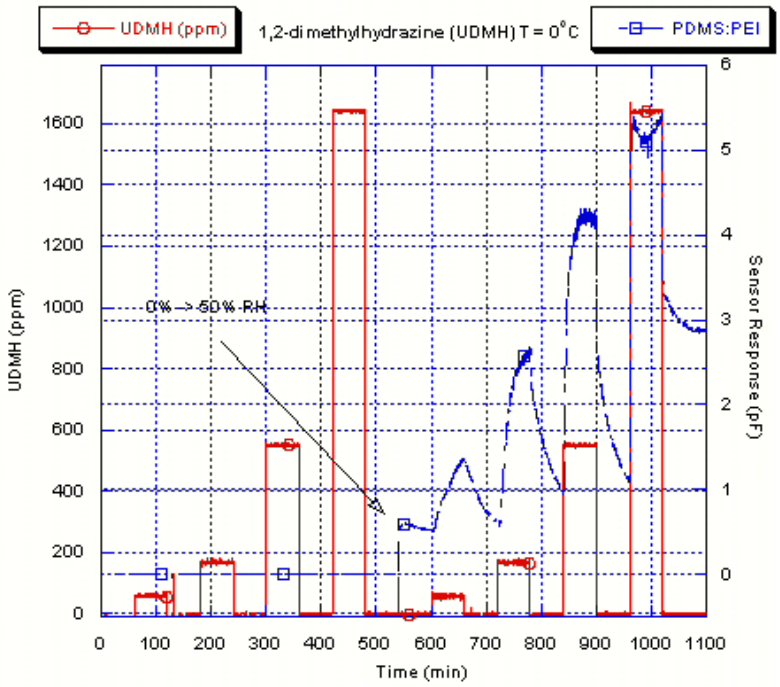


**Figure 28**. Response of composite sensor to UDMH under low (~0%) and high humidity (LOD ~0.26 ppm).

With the dry carrier gas, no signal is observed even at high UDMH concentration (~ 1650 ppm); increasing the humidity to 50%, a strong signal is observed even the lowest concentration (~If the material consisted only of silica, a proton transfer would be thermodynamically favored with the $pK_a$ of the silanol ~4.5 and the $pK_a$ of the hydrazinium ion ~ 8 (see F. G. Bordwell *Acc. Chem. Res.* **1988**, *21*, 456, 463)). However, with the composite nature of the sensor, it seems unlikely that bare Si-OH groups are on the sensor surface. Futhermore, the PAPPS material and the PEI contain primary amines that would also participate in any proton transfer. The dependence of the signal upon the humidity is also somewhat puzzling. One explanation is that with dry carrier gas (compressed air), all the hydrazines 'stick' to surface of the test system and the water simply acts as a carrier for the hydrophilic fuels. Another hypothesis is that the water 'activates' the sensor surface towards the detection of the unsubstituted and substituted hydrazines. Regardless of the mechanism involved, the dependence of the signal upon the presence of water will be an advantage for applications of hydrazine detection in humid environments (i. e. shipboard monitor for PEL determination) for the detection of hydrazine in the missile and the canister the necessary detection limit are orders of magnitude high which may allow us to detect using these materials (cf Figure 20).

To detect the oxidizers, we narrowed our selection to nitrogen tetroxide (NTO) due to guidance received during the Phase I contract. Due to the health and safety hazard of NTO we took advantage of the equilibration of NTO in air (Equation 2).

$$N_2O_4 \rightleftharpoons 2NO_2 \qquad \text{(eq 2)}$$

Thus we obtained a dilute sample of $NO_2$ in nitrogen (5000 ppm )[14] and exposed the chemoselective materials to varying concentrations of $NO_2$. Initial results indicated that PECH is the most sensitive chemoselective materials to nitrogen dioxide (Figure 29).

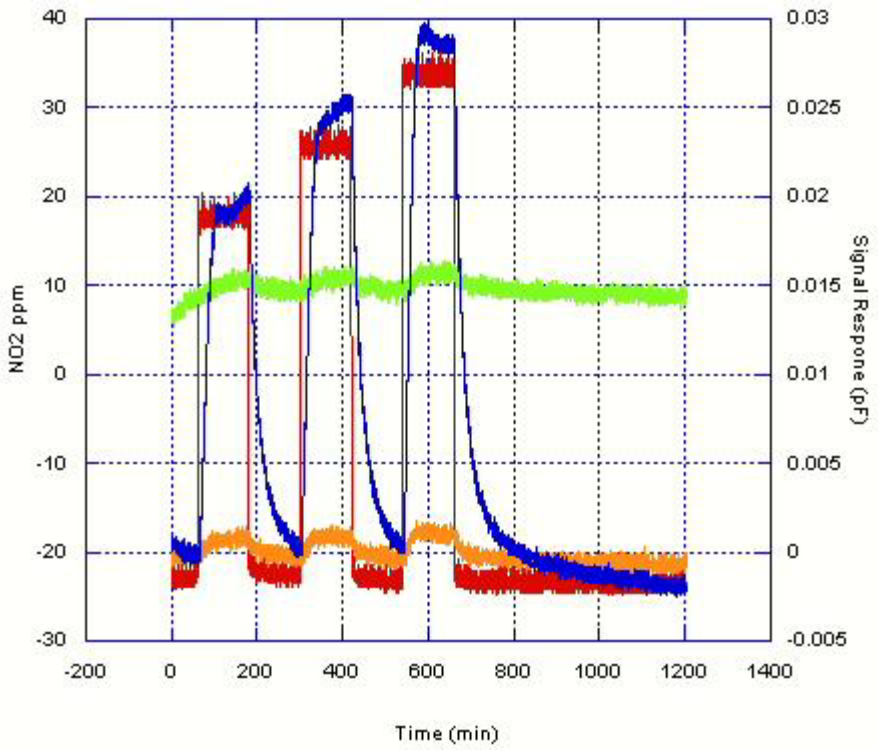


**Figure 29** Sensor Response to $NO_2$ (0% RH, T = 25ºC) Key: $NO_2$: red; PDMS:PEI:PAPPS: orange; PECH; blue SXFA: green

The high sensitivity of PECH to $NO_2$ was rather unexpected and must be due to a dipole-dipole or Van der Waals interaction. We have recently observed similar sensitivity of PECH to nitroalkanes and nitroaromatics. The other materials that showed sensitivity to $NO_2$ were the metal centered substituted phthalocyanines (Figure 30)

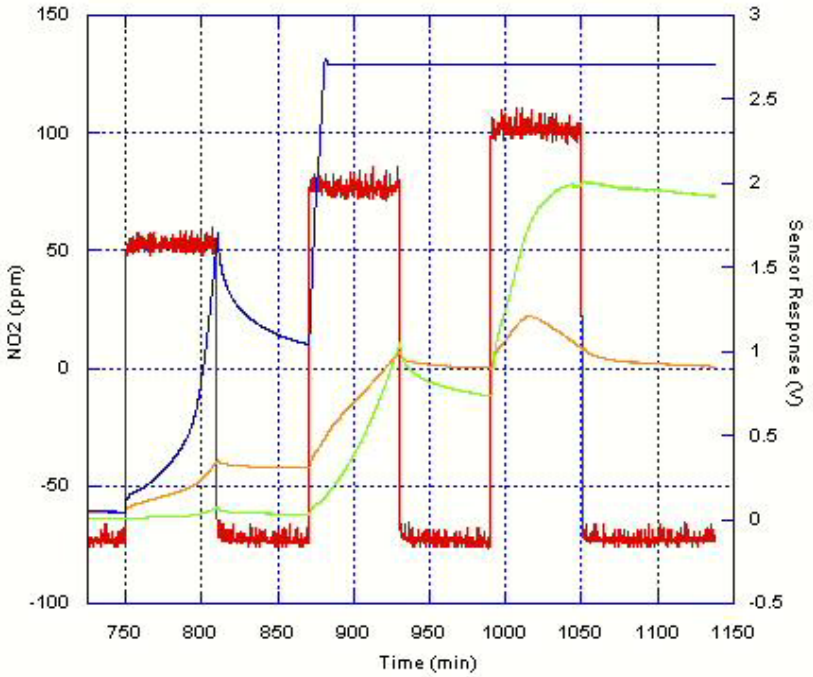


**Figure 30** Sensor Response to $NO_2$ (0% RH, T = 25ºC) Key: $NO_2$: red; Co(II)tBuPc: orange; Ni(II)tBuPc; blue Cu(II)tBuPc: green

In contrast to the reversible interaction of $NO_2$ with PECH, SXFA, and PEI:PDMS:PAPPS, the interaction of nitrogen dioxide with all the metalphthalocyanine was irreversible and in some cases caused a large enough response to "short" or rail the readout system (Ni(II)tBuPc) indicating a chemical change to the material (perhaps oxidation of the metal center). This interaction is a possible topic of study for Phase II, since the large response may be exploited to develop a high sensitivity component to the sensor system, or a dosimeter-type sensor product.

From the data gathered in Phase I, the current choice for a sensor array to detect the fuels and allow for the filtering of interferrent combines previously characterized materials along with novel materials synthesized and characterized during the 6-month contract (Table 3).

**Table 3.** Phase I Selection of Chemoselective Materials for 1st Generation Hypergolic Chemical Detection[a]

| Agent Class | Chemical | LOD (ppm) | Candidate Polymers[a] |
|---|---|---|---|
| **Hypergolic Fuels** | Hydrazine | 16.3 | PEI:PDMS:PAPPS |
| | Monomethyl Hydrazine | 0.3 | |
| | Dimethyl Hydrazine | 0.26 | |
| **Oxidizers** | nitrotetroxide ($NO_2$) | 0.27 | PECH, |
| **Interferents** | Ethanol | 12 | Au-C2-nBuEster |
| | Acetone | 17 | HC |
| | Octane | 5 | Au:C12-H |
| | Humidity | 1% | Au:C12:COOH |

[a]see Table 2 for structures

A chip containing the aforementioned materials or functional equivalents will be coated and tested during Phase II of this contract.

**Task 2. Hardware Systems Development**

*Redesign of motherboard for low power requirements and small size.* Seacoast Science's pre-existing motherboard (SC100) has been analyzed and redesigned for improved system performance (reduced noise, increased speed, easier communication with radio circuit) (**Figure 31, 32).**

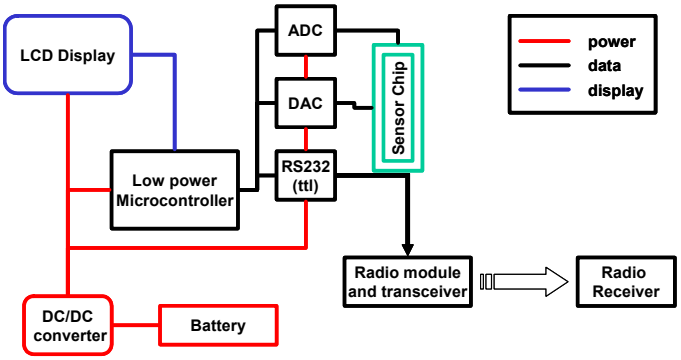


**Figure 31**. System schematic

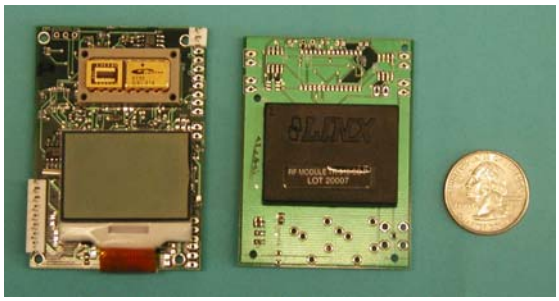

**Figure 32**. Photograph of prototype motherboard (left) and radio transmitter board (right) next to a quarter.

As part of the prototype development process, the optimizations to the sensor readout and supporting electronics have been started. We compared the old GS1 (Seacoast's first generation circuits) and new SC200 Motherboards (produced in 2005) with following results.

*Autoranging Capabilities:* Initial comparison tests showed that the two motherboards generally produced similar signal to noise ratios (SN). However the SC200's ability to autorange (alter board voltages to maximize sensor response while sensing) produced larger SN ratios under specific test conditions. These conditions include exposure to analytes that elicit large changes in the capacitance/voltage of the polymer coated sensors on the daughterboards. Under these circumstances the older GS-1 boards would "rail" or reach maximum sensor voltage, at which point

they would no longer be sensing additional upward changes in analyte during tests. The autoranging capabilities of the SC200 coupled with the shift from voltage to capacitance when reading sensors has allowed us to increase the sensor range for our chips. In similar test circumstances the SC200 boards continued sensing at analyte exposure levels past the capabilities of the GS1 to sense.

*Manual Tuning Capabilities:* Both GS-1 and SC200 boards would have reduced SN ratios under circumstances where the capacitive value of the coated chemoreceptor on the sensor chip was extremely low, as defined by the polymer chemistry of the coating. In the GS-1 this was solved by manually adjusting chip voltages to bring voltage values back into the normal range. Our engineers have published a new software control set for the SC200 board, giving us the ability to tune the SC200 in an identical fashion to the GS1. This has allowed us to continue to test a wide variety of polymer compounds no matter what hardware is being used.

*Sampling Rates and S:N ratio*
When the over-sampling rate for both boards was held constant, the newer SC200 boards demonstrated higher SN ratios than the old GS-1 boards. The default over-sampling rate for the GS1 boards was 128, while the SC200 boards were set at 16. In initial comparisons, the boards were tested using default values and they produced similar SN ratios. When both boards were set to 128, the SC200 outperformed the GS-1 in SN ratio comparisons by several orders of magnitude. Over-sampling is directly related to power consumption in these systems and these results indicate that progress is being made towards our goal of producing extremely low power consumption sensors while maximizing SN ratio.

Based on these results we will be assembling during Phase II 20 new motherboards for use in laboratory testing and in prototypes**.**

*Sampling/Preconcentration System:*
*First Generation Seacoast Science Miniature Sampling System*

A brass board layout of the Seacoast Science preconcentrator system (Figure 33) has been integrated with our MEMS capacitive sensors and has the following features:

- 6 inch length and 1/8 inch diameter preconcentrator tube
- Tenax or other absorbent packing
- Pump that pulls from 25 ml/min to 200 ml/min through the system depending on length of capillary tubing
- Tube heats to 200°C in approximately 90 seconds
- Capillary column of various lengths
- Small sampling pump

Using this “trap and purge” preconcentration system we are able to conduct concentration studies with our chemicapacitors as detectors. The sample is collected on a preconcentrator; the heater is thermally cycled releasing a slug of material into the capillary column that separates the analytes, the capillary output flows over the sensor array. The motherboard and sampling pump are also present.

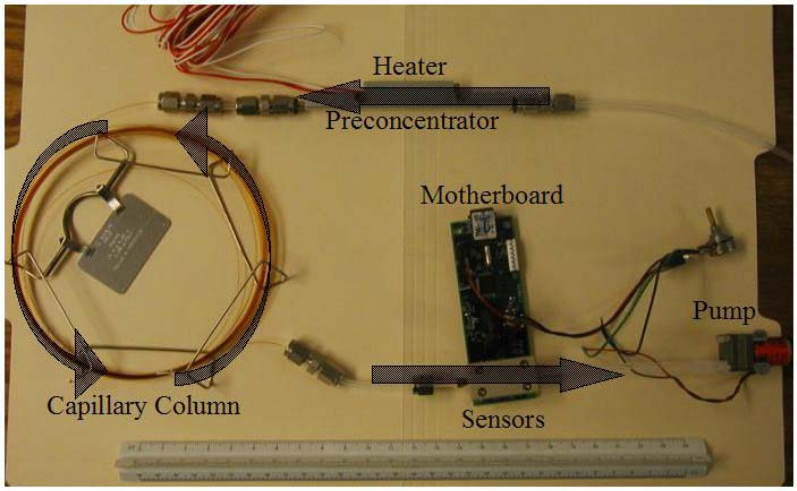

**Figure 33**: Layout of the Seacoast Sample Handling System. The Arrows Indicate the Flow Path.

Seacoast Science has recently licensed the technology associated with a micro-machined preconcentrator co-developed at the Naval Research Laboratory called CASPAR (Cascade Avalanche Sorbent Plate ARray). It can be used to selectively trap analyte(s) of interest and thermally desorb a narrow time width pulse of concentrated analyte into a narrow orifice intake (Figure 34).

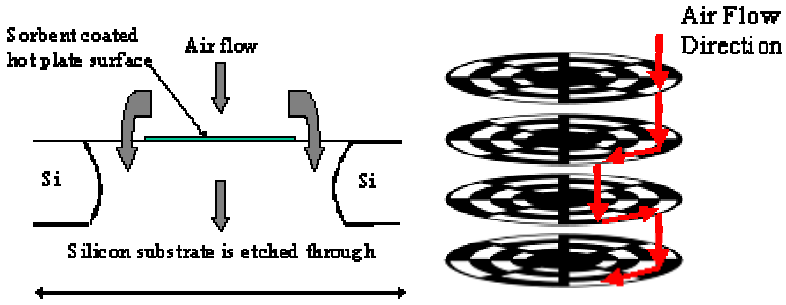


**Figure 34**. CASPAR Preconcentrator Concept

The design of CASPAR provides a high surface area "collection plate" with an extremely low-pressure drop, to allow a high flow to be passed through the device and intimately contact the majority of the collection surface, with the minimum power expended. During a scheduled working meeting at the Navel Research Laboratory (August 2005) the integration of their CASPAR preconcentrator with Seacoast Science's sensor technology was further investigated. Using PECH and Adiol and the IDT architecture, detectable preconcentration of diispropylmethylphosphonate (DIMP) was observed (Figure 35)

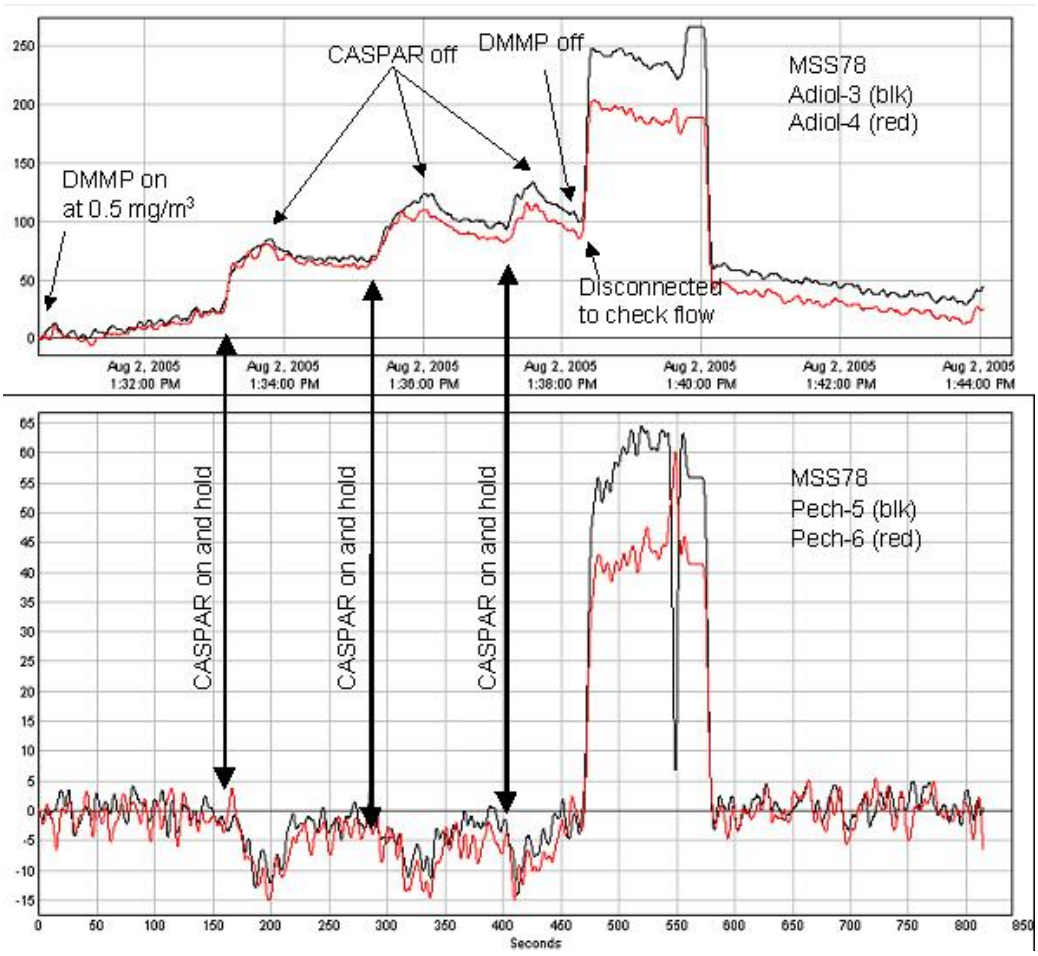


**Figure 35**. CASPAR Preconcentration of DIMP

Further tests with the CASPAR unit may be accomplished during Phase II. Finally, the design and construction of a novel preconcentrator was accomplished during Phase I. Preliminary tests of our new system (Figure 36) demonstrated detectible concentration of DIMP when the wire was dip-coated with the functionalized polycarbosilane HC. This can then be employed in a low volume chamber to increase the sensitivity of our sensor. Some feature of our first generation preconcentrator:

- Small size: less than 1 cubic centimeter
- Fast heating: From 25 to 150 deg C in 2 sec.
- Heat is applied directly to substrate.
- Low thermal mass means low power.
- 10 and 3 mil gauge nichrome wire.

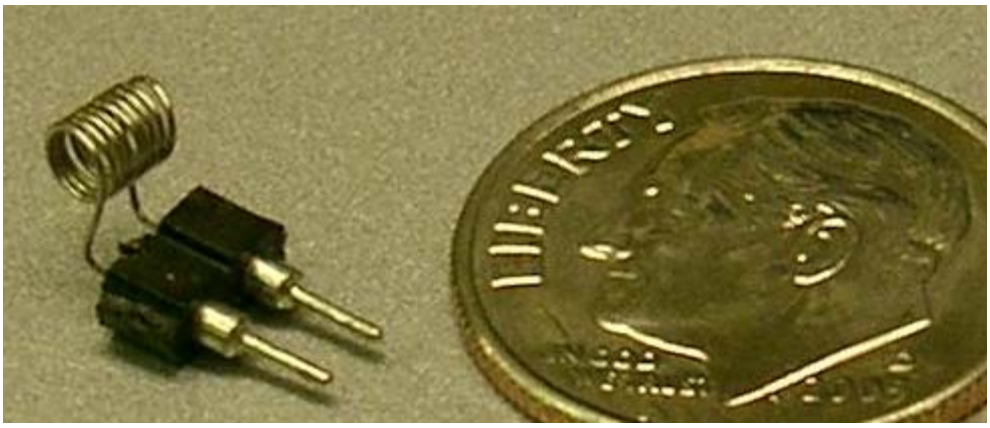

**Figure 36**. Heated Sensor Element Coated With A Chemoselective Material Coating HC.

**Task 3. Software Systems Development**: *Design a software algorithm capable of measuring outputs from the chemicapacitive sensors, temperature sensor, and humidity sensor*

Based on previous findings about the various pattern recognition algorithm options commercially available, our collaborators at the University of Maine concluded that Matlab was found to contain most of the necessary functions required for the pattern recognition in this project. Dr. Segee's team analyzed the data, created an algorithm that started by identifying the principal components of the data then used these components as the new sensors, and fed the data to a simple neural network.

As a first step, a sensor data set containing data for exposures to kerosene, diesel, toluene and unleaded gasoline was sent to Dr. Segee's team. The data were analyzed and an algorithm was created that started by identifying the principal components of the data. These components were used as the input data to a simple artificial neural network (ANN). The results (Figure 37) show that they could identify the 4 chemicals in the data set, with some "mis-identification" during transitions. Based on this data we have established a more complete comprehensive test plan for collecting the future training data.

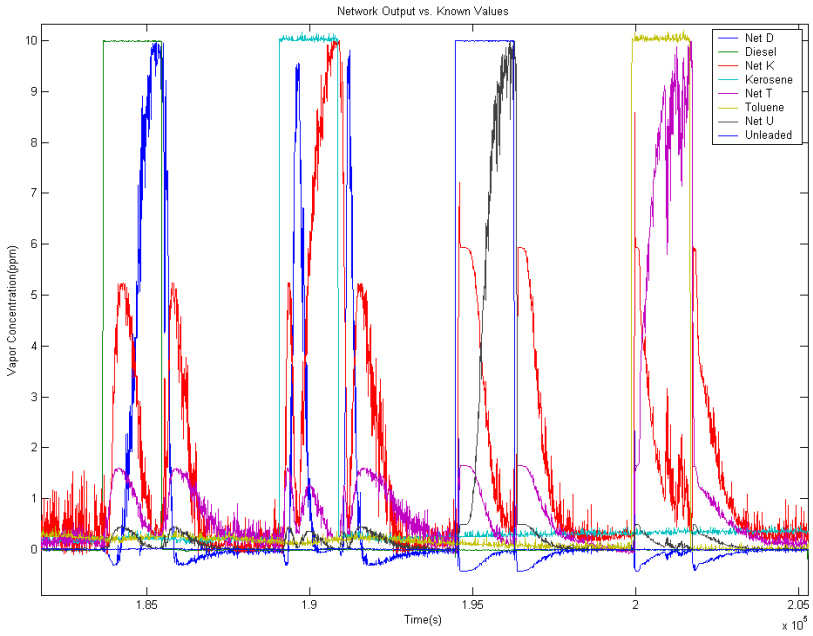


**Figure 37.** PCA/Neural net results for the first data sets. The "square" traces are the actual settings of our vapor delivery system. The "Net" traces are the results of the algorithm. In each case (Diesel, Kerosene, Toluene, & Unleaded Gas) the chemical is identified correctly as the response reaches equilibrium. For this data set, all chemicals were dosed at the same partial pressure. The classification was accomplished without preconcentration.

From the graph, one can observe that there is some false identification during the beginning and end of each exposure. However, when viewed from a single exposure standpoint, an integrating competitive function would easily determine which gas was present. This is possible because the dominant signal in each exposure corresponds to the vapor present. Once the appropriate gas was identified it could be possible to examine the response of that single output of the network to determine concentration.

We propose to pursue this avenue of data processing to mitigate the known interferents and environmental variables: temperature, humidity, environmental contaminants, etc. The promising results from such similar vapors suggest that the environmental variables should be easier to separate from response of the hypergolic compounds. Humidity and temperature sensors that do not sense the compounds of interest will provide independent or "orthogonal" sensor responses improving the system selectivity.

The sensor data collected in Phase I show a repeatable response of individual sensor elements, low-drift, and reasonable linearity. Furthermore, although the sensor films show responses to a variety of target gases, the cross-sensitivities are sufficiently different to allow discrimination of various analytes. In general, when a large number of sensors are used to determine the concentration of a number of target gases, the problem quickly becomes extremely complex. Although the sensors are temperature and humidity dependent, we can obtain an accurate estimate of both dependent variables and compensate for their effect on sensor response. Software algorithm development will continue in Phase II.

**Task 4 Based on the Phase I test results complete and document the design of an inexpensive detector system that will meet all requirements for a hypergolic chemical detection system capable of being used after further development in Phase II.**

***Radio Integration*.**

A Linx Technologies, Inc. system transceiver was selected in the SC-R-915 radio module based on preliminary laboratory test results using an evaluation kit, operating voltage compatibility with the SC-200, power requirement and channel availability. A low power microcontroller was added to the circuit to process the sensor data. The microcontroller provided a custom designed, error correction protocol compatible with our SC-200 sensor data stream. A test of the range and error rate of the transceiver with very low data rate was performed in our lab and found to be satisfactory.

The supporting circuitry, for the transceiver unit and data packetizer was designed, and the entire radio module fit into a small area measuring 1.5" x 2.5". Currently, the radio module is designed to use the battery directly from the SC-200 unit or any other sensor package with no less than 3.0V dc power. This system is designed for purposes of demonstration, and will act as a point-to-point radio. During phase II of this program, the firmware of the radio will be upgraded to handle a multi-sensor wireless data network and increase the error control and security features. A modular design approach to the radio was adopted at this phase, allowing the performance of both the radio and the sensor module to be optimized individually. Both modules can be integrated onto a single PCB during the final phase of the Phase II program.

***Prototype Development***

From the development work on radio integration and power optimization, we designed and fabricated a prototype point detector (Figure 38) that upon preparation of a prototype sensor array (cf Table 3) will be capable of detection of hypergolic compounds during Phase II.


**Figure 38**. Seacoast Science Prototype Hypergolic Chemical Detector Detector.

The black unit in Figure 38 contains the sensor array and (SC200) circuits, a sampling pump, and a COTS 9 Volt battery, while the unit with the blue overlay contains the user interface (button operated menu system) and Linx radio for wireless communication. For prototyping purposes these systems were made modular, however, these components can be easily combined into one unit, with the circuits placed on one PC board to reduce the overall size and weight.

1 Snow, A.W.; Wohltjen, H.; Jarvis, N.L.; *NRL Review* **2002**, 45.

2 Brust, M.; Walker, M.; Bethell, D. Schiffrin, D. J.; Whyman, R. *J.. Chem Soc. Chem. Commun.* **1994**, 801-802

3 Synthesized in a similar fashion with tetra(*n*-butyl)ammonium bromide as the phase transfer catalyst.

4 COOH and C6 OH functionalized Au nanoparticles have been previously reported using a different synthesis method. See Shi, W.; Sahoo, Y.; Swihart, M. T. *Colloids and Surfaces A. Physiochem. Eng. Aspects* **2004**, *246*, 109-113

5 Patel, S. V.; Mlsna, T. E.; Fruhberger, B.; Klaassen, E.; Cemalovic, S.; Baselt, D. R. *Sensors and Actuators B: Chemical*, **2003**, *96*, 541-553.

6 (a) McCorkle, D. L.; Warmack, R. J.; Patel, S. V.; Mlsna, T.; Hunter, S. R.; Ferrell, T. L.. *Sensors and Actuators B - Chemical*, 2005, *107* 892-903. (b) Mlsna, T.E.; Mowery, R.; and McGill, R.A. "The Design of Aromatic Silicone Polymers and their Evaluation as Sorbent Coatings for Chemical Sensors," in *Silicones in Coatings*, 1998.

7 (a) Kriner, W. A. *J. Org. Chem.* 1964, *29*, 1601-1605. (b) Whitmarsh, C. K.; Interannte, *Organometallics*, 1991, *10*, 1336-1344. (c) Whitmarsh, C. K.; Interannte, L. Y. *United States Patent*, 5,153,295, October 6, 1992. (d) McGill; R. A.; Houser; E. J.; *United States Patent* 6,617,040, September 9, 2003. (e) McGill; R. A.; Houser; E. J.; Mlsna; T. *United States Patent* 6,630,560, October 7, 2003. (f) McGill; R. A.; Houser; E. J.; *United States Patent* 6,660,230, December 9, 2003. (g) Houser; E. J.; McGill; R. A. *United States Patent Application* **2004/0058057 A1**, March 25, 2004

8 (a) Litt, M. H.; Schmitt, G. J. *United States Patent No.* 3,324,187, June 6, 1967. (b) Urry *J. Org. Chem.* 1968, *33*, 2302-2310.

9 Roebuck, A.; Adkins, H. *Organic Syntheses, Coll. Vol*. 3, 217

10 Brinker, C. J.; Scherer, G. W. *Sol-Gel Science : The Physics and Chemistry of Sol-Gel Processing*, Academic Press, San Diego, CA 1989.

[11] Personal communication, William Trogler

[12] Gold nanoparticles Au:C11:COOH and Au:C6:OH have been previously reported using a different synthetic method. See Shi, W.; Sahoo, Y.; Swihart, M. T. Colloids and Surfaces A. Physiochem. Eng. Aspects 2004, 246, 109-113

[13] For all limit of detection (LOD) calculations the following equation is used: $LOD = \frac{3 \times noise * conc(ppm)}{signal}$

[14] Obtained from Scott Specialty Gasses, Plumsteadville, PA 18949